REVIEWS OF GEOPHYSICS, VOL. 24, NO. 2, PAGES 439–468, MAY 1986

Earth Radiation Budget Data and Climate Research

D. L. HARTMANN,[1] V. RAMANATHAN,[2] A. BERROIR,[3] AND G. E. HUNT[4]

An overview is presented of the uses of top of the atmosphere radiation budget measurements in studies of climate. The net radiative energy flux at the top of the atmosphere must be balanced by local heat storage in the earth-atmosphere column or by horizontal transport in the atmosphere and ocean. Regional variations in the components of the radiation balance are significant and place important constraints on regional and global climate. If suitable time averaging is applied, regional net radiation can be used to infer horizontal transport of energy in the atmosphere and ocean. Estimates of equator-to-pole transport in the atmosphere and ocean based upon currently available top-of-atmosphere radiation budget measurements contain unacceptably large uncertainties associated with uncertainties in the radiation budget measurements themselves. Diurnal and interannual variations in regional radiation balances are large and important but have not yet been properly sampled with broadband instruments. Both have the potential for providing important insights into climate. The role of cloudiness in climate sensitivity remains one of the major uncertainties in quantitative estimates of climate changes associated with particular perturbing influences. Radiation budget data can be used to estimate the effects of actual cloudiness on the top-of-atmosphere heat balance and the dependence of these effects on location and season. The observational studies of the effect of cloudiness on the radiation balance at the top of the atmosphere that have been completed to date all suffer from one or more of three fundamental problems. These are that the parameters of the cloudiness are not accurately known, the radiation budget data are not based on measurements whose frequency response is unbiased in relation to the emissions of the sun and the earth, and the diurnal sampling of the measurements is not complete. The uncertainties associated with each of these problems are expected to be reduced as a result of analyses based on data from the Earth Radiation Budget Experiment. In order that quantitative estimates of climate change be as accurate as possible the general circulation models (GCMs) which produce these forecasts must be critically evaluated with observed data. Many of the most important mechanisms for perturbing climate (e.g., CO_2, volcanic aerosols, surface albedo changes) and many of the most important feedback processes (e.g., relative humidity feedback, cloud feedback, ice-albedo feedback) directly involve the radiation balance at the top of the atmosphere and its relation to surface climate. Since the radiation balance at the top of the atmosphere can, in principle, be measured very accurately from space, it is natural that the simulation of top-of-atmosphere energy fluxes by GCMs should be carefully validated against observations. Because of the complexities introduced by clouds, a complete validation of the radiation budget of a GCM is a long and difficult task. A strategy is suggested here in which the clear-sky fluxes of the model are first compared with a clear-sky radiation budget climatology derived from observations. The radiation budgets with clouds included can then also be compared. This procedure should isolate problems not associated with cloudiness and indicate whether, in the grossest sense, the model clouds are correctly influencing the radiation balance. Comparisons between instantaneous synoptic maps of the radiation budget components and numerical forecasts can also be used to diagnose the performance of models.

CONTENTS

[1]Department of Atmospheric Sciences, University of Washington, Seattle.
[2]Climate Sensitivity Group, National Center for Atmospheric Research, Boulder, Colorado.
[3]Institut National des Sciences de l'Univers/CNRS, Paris.
[4]Centre for Remote Sensing, Imperial College of Science and Technology, London.

Paper number 5R0784.
8755-1209/86/005R-0784$15.00

1. INTRODUCTION

The total radiative energy flux at the top of the atmosphere constitutes the most important exchange between the earth and its environment. It is necessary to understand the relationship of the top-of-atmosphere radiative energy fluxes to the earth's climate to obtain, for example, accurate predictions of the effects of increasing atmospheric carbon dioxide on the surface climate. An important step toward understanding this relationship is to measure the top-of-atmosphere radiative energy fluxes, the radiation budget components, with sufficient accuracy, spatial resolution, and temporal resolution.

This paper reviews the use of observations of the radiation budget components at the top of the atmosphere in scientific studies of the earth's climate. Particular attention is given to problems for which data from the Earth Radiation Budget Experiment (ERBE) are expected to be especially helpful. The instrument accuracy and the spatial and temporal sampling of the ERBE measurement system are expected to surpass those of any previous attempts to measure the earth's radiation budget (ERB), and a number of investigations are planned which will take advantage of the unique features of the ERBE data set. Other reviews of radiation budget studies can be

TABLE 1. Globally and Annually Averaged Radiation Budget Components From a Number of Sources Rounded to the Nearest Integer

Source	Albedo, %	Long-Wave Emission, W m^{-2}
Pre-1972 experiments [*Ellis and Vonder Haar*, 1976]	30.4	236
Pre-1972 experiments plus Nimbus 6 ERBE [*Campbell and Vonder Haar*, 1980]	30	232
Nimbus 6 ERB wide field of view [*Jacobowitz et al.*, 1979]	31	234
Nimbus 6 ERB narrow field of view [*Campbell and Vonder Haar*, 1980]	31	230
Nimbus 7 ERB wide field of view	31	229
Nimbus 7 ERB narrow field of view	33.1	233
NOAA scanning radiometers [*Ohring and Gruber*, 1983]	31	244
Best estimate	30.5 ± 1	233 ± 5

Adapted from *Jacobowitz et al.* [1984].

found in the works by *Stephens et al.* [1981], *Kandel* [1983], *Ohring and Gruber* [1983], and *Vonder Haar* [1983].

The body of this paper is divided into three main sections. Section 2 reviews previous scientific studies of regional energy balances and points out the need for more accurate ERB data in studies of this type. A subsection illustrates the importance of diurnal variations in broadband fluxes, which will be adequately sampled for the first time by the ERBE system of two sun-synchronous satellites and one 57° inclination satellite whose orbit will precess through all local times.

Section 3 focuses on the use of ERB data in observational studies designed to elucidate the role of clouds in the maintenance of the current climate and their potential influence on the sensitivity of the current climate. Previous studies are first critically reviewed and then followed by suggestions for improvement and an indication of how ERBE data are expected to assist in refining studies of this type.

The utilization of ERB data in theoretical and model studies is treated in section 4. The discussion here is confined primarily to the use of ERB data in the development of the most complex models of the general circulation. These are the models used for detailed climate simulations and for extended range numerical weather forecasting. Several specific strategies for effectively using ERB data to test these models are set out.

Two short sections are included at the end of the paper. Section 5 emphasizes the considerable scientific opportunities afforded by the coincidence in time of the Earth Radiation Budget Experiment and the International Satellite Cloud Climatology Project (ISCCP). Section 6 describes the nature of the solar constant data to be provided from the solar constant monitor included in the ERBE instrument package.

2. Regional Energy Balances

Introduction

The net radiative energy exchange at the top of the atmosphere is the primary component of the energy balance of the earth-atmosphere system and is a central determinant of the earth's climate. For a particular region one may write the energy balance for the earth-atmosphere system as

$$\partial E/\partial t = R - \text{div } \mathbf{T}_A - \text{div } \mathbf{T}_O \quad (1)$$

Here E is the total amount of energy in the earth-atmosphere within a particular region, R is the net radiative energy flux at the top of the atmosphere coming into the region of interest, and div $\mathbf{T}_A$ and div $\mathbf{T}_O$ are the fluxes of energy leaving the region horizontally as a result of atmospheric and oceanic transport, respectively. All of these terms are usually divided by the area of the region of interest and hence have units of watts per meter squared. The net radiation can be written

$$R = S - F \quad (2)$$

where S is the absorbed solar radiation and F is the outgoing long-wave emission from the earth-atmosphere. The planetary albedo α_p is defined by the relation

$$S = S_0(1 - \alpha_p) \quad (3)$$

where S_0 is the incident solar flux at the top of the atmosphere.

Global Averages

When the region considered includes the entire earth's surface, the horizontal transport terms drop out of (1), which becomes

$$\partial E/\partial t = R \quad (4)$$

If an average is taken over a sufficiently long time, for example, over an integral number of years, the tendency is expected to be small, and (4) simplifies further to

$$R = S - F = 0 \quad (5)$$

The requirement that the net radiation be small when averaged over the area of the earth and over a year provides a check on the accuracy of a radiation budget measurement system. In addition to the degree of attainment of the expected balance the values of globally and annually averaged planetary albedo and outgoing long-wave flux are of interest in themselves. Table 1, adapted from *Jacobowitz et al.* [1984], shows planetary albedo and long-wave flux taken from a number of sources. The numbers provided are fairly consistent with each other except for the albedo from the Nimbus 7 ERB scanner and the long-wave emission from the National Oceanic and Atmospheric Administration (NOAA) scanning radiometers. *Jacobowitz et al.* [1984] have suggested that the high albedos derived from the Nimbus 7 ERB scanner may be due to an overrepresentation of high albedos obtained at large scan angles. The NOAA long-wave estimates are based on observations from a narrow spectral interval centered in the 11-μm window region [*Gruber and Winston*, 1978]. The large outgoing long-wave flux derived from NOAA measurements appears to result from an imperfect narrow spectral band to broadband conversion algorithm.

Annual Variation of Global Means

Over the course of a year the global mean insolation, planetary albedo, and long-wave emission vary. These variations are large enough to be measured with current observing systems. Figure 1 shows the annual variation of net radiation, long-wave radiation, and planetary albedo derived from several data sets. While the detailed behavior varies, the basic characteristics of the annual variations in global mean quantities are the same in the data sets shown.

The solid line in the top panel of Figure 1 shows the deviation of the top-of-atmosphere insolation from its annual mean. The annual variation results from the eccentricity of the earth's orbit. At present the earth is closest to the sun near the time of the December solstice, and the solar flux density is greater during that season.

Net radiation also shows a significant annual variation of

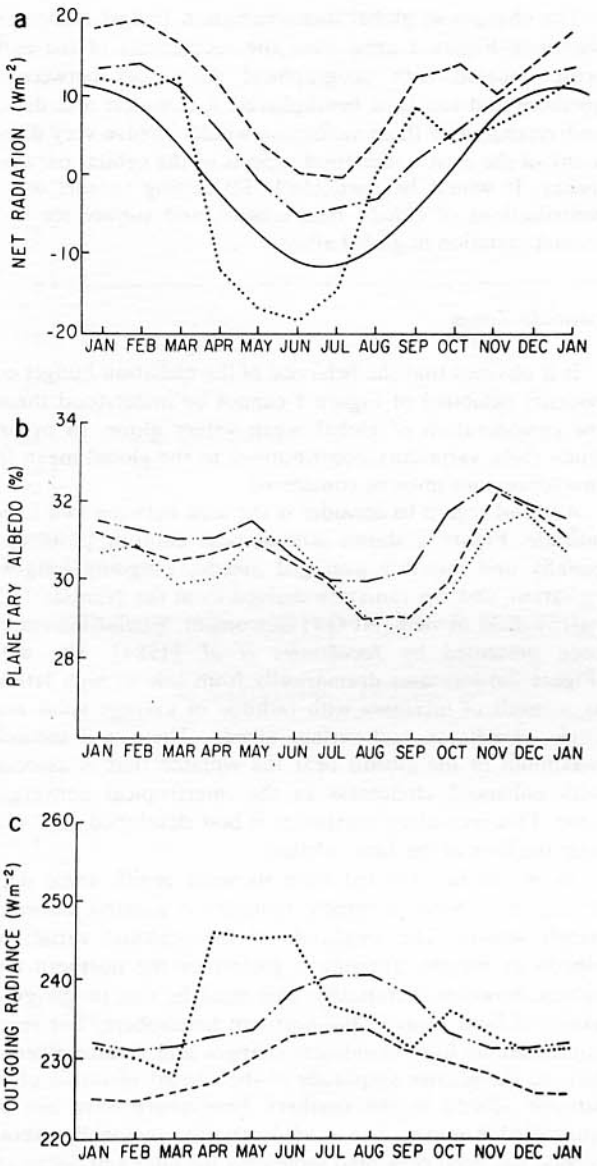

Fig. 1. Annual variation of globally averaged (*a*) net radiation, (*b*) planetary albedo, and (*c*) outgoing long-wave exitance based on data from *Ellis and Vonder Haar* [1976] (dotted curves), Nimbus 7 ERB wide field of view (WFOV) (dashed curves), and Nimbus 6 ERB WFOV (dotted-dashed curves) (adapted from *Slingo* [1982] and *Jacobowitz et al.*, [1984]). The solid curve in Figure 1*a* indicates the magnitude of the deviation from the annual mean insolation due to the earth's eccentricity.

about 20 W m^{-2} peak to peak amplitude with the maximum net radiation occurring in the vicinity of the December solstice. This is in phase with and about the same amplitude as the current annual variation of the incoming solar radiation at the top of the atmosphere.

The planetary albedo reaches a maximum global mean value of about 32% near the time of the December solstice. There is a suggestion of a secondary maximum near the June solstice and a sharp minimum near 29% just before the September equinox. This albedo variation reduces the effect on the net radiation of the annual variation in incoming solar radiation that results from the eccentricity of the earth's orbit around the sun.

The annual variation in long-wave emission has a peak to peak amplitude of about 9 W m^{-2} with the largest values occurring in the June–August period. This annual variation results from the greater surface area occupied by dry continental areas in the northern hemisphere. During summer the surface temperatures in these areas increase, and this temperature increase results in a larger long-wave emission. Ocean temperatures vary much less with season, and the change in long-wave emission is correspondingly small. Over wet continental areas, variation in clouds can modulate annual variations in long-wave emission. Data presented by *Oort* [1983] show a rather large annual variation in global mean surface temperature which has the same root cause as the annual variation in outgoing long-wave radiation. The global mean surface temperature is highest in July (16.7°C) and lowest in January (13.1°C). This annual variation in global mean surface temperature is dominated by the large annual cycle over the northern hemisphere continents.

It is interesting that while the annual variation in net radiation is similar in amplitude and phase to the annual variation in incoming solar radiation, the manner in which this comes to be is not straightforward. The annual variation in absorbed solar radiation is smaller by half than the annual variation in available insolation because the global mean albedo increases when the insolation does. The annual variation in outgoing long-wave radiation is as large as that of absorbed solar radiation but is 180° out of phase with it. The result is an annual variation of net radiation which is twice as large as it would be if the outgoing long-wave radiation were constant through the year.

The annual variation of globally averaged insolation due to the eccentricity of the earth's orbit provides a forcing to the climate system. The change in radiation budget components resulting from this forcing is in part a measure of the response of the climate to this forcing and in part a response to the different geography of the two hemispheres. This response, particularly the albedo response, is not well understood. Indeed, it appears that the magnitude of the signal is close to the limit of our ability to measure. More precise global measurements, such as those expected from ERBE, coupled with global data on cloudiness that will be produced by the International Satellite Cloud Climatology Project will provide the opportunity to investigate these annual variations in global mean radiation budget components.

A complete understanding of these variations would be an important step toward understanding climate sensitivity and change. Paleontological evidence suggests that variations of the earth's orbital parameters play an important and perhaps central role in determining the succession of glacial and interglacial epochs which have occurred over the last million years [*Hays et al.*, 1976]. Periodicities appear in the record of global ice volume corresponding to the 20,000-year periodicity in longitude of perihelion, the 40,000-year periodicity in obliquity, and the 100,000-year periodicity in eccentricity. The global ice volume can be hindcasted statistically with surprising accuracy using only the earth's orbital parameters as input [*Imbrie and Imbrie*, 1980]. The basic mechanism whereby the orbital parameters can influence the climate was first set down by *Milankovitch* [1920]. Since only the eccentricity influences the annually and globally averaged insolation and then only by a very small amount, the orbital parameter theory hypothesizes that the climate is sensitive to the distribution of insolation with latitude and season, which varies locally by as much as 30% as a result of orbital parameter changes. Because albedo changes associated with snow and ice cover are thought to provide an important positive feedback mechanism, and perennial ice forms most easily over land, attention has focused on the summertime insolation in high latitudes of the northern hemisphere.

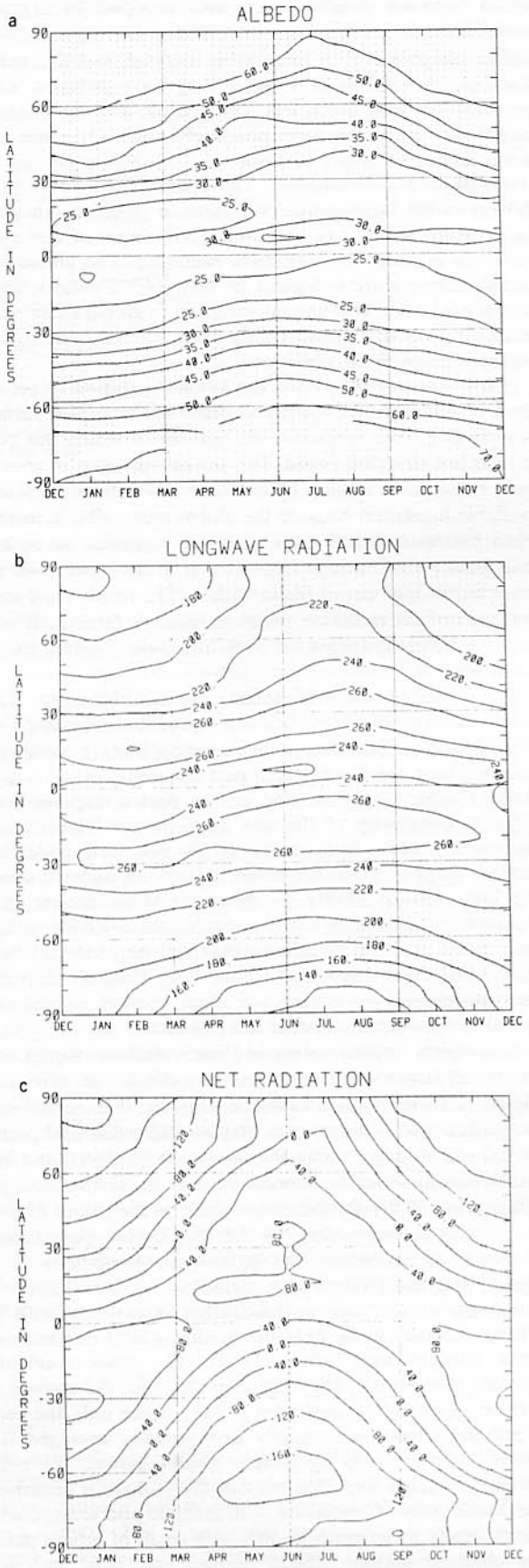

Fig. 2. Latitude-time contour plots of (*a*) albedo (contour interval 5% up to 50 and 10% above 50; values greater than 30% are shaded), (*b*) outgoing long-wave radiation (contour interval 10 W m^{-2}; values less than 220 W m^{-2} are shaded), and (*c*) net radiation (contour interval 20 W m^{-2}; negative values are shaded) based on the Nimbus 7 ERB NFOV instrument.

The changes in global mean radiation budget components shown in Figure 1 arise from the eccentricity of the earth's orbit, coupled with geographical differences between the northern and southern hemispheres. A complete and detailed understanding of these variations would involve very directly many of the least understood aspects of the orbital parameter theory. It would be particularly interesting to sort out the contributions of clouds, land albedo, and surface ice to the annual variation in global albedo.

Latitude Zones

It is obvious that the behavior of the radiation budget components exhibited in Figure 1 cannot be understood through the consideration of global mean values alone. In order to study these variations, contributions to the global mean from smaller regions must be considered.

A useful region to consider is the area between two lines of latitude. Figure 2 shows latitude-time contour plots of the zonally and monthly averaged albedo, outgoing long-wave radiation, and net radiation derived from the Nimbus 7 ERB narrow field of view (NFOV) instrument. Similar figures have been presented by *Jacobowitz et al.* [1984]. The albedo (Figure 2*a*) increases dramatically from low to high latitudes as a result of increases with latitude of average solar zenith angle, cloudiness, and surface albedo. There is a secondary maximum in the albedo near the equator that is associated with enhanced cloudiness in the intertropical convergence zone. This secondary maximum is best developed at 5°–10°N near the time of the June solstice.

As would be expected from its solar zenith angle dependence, the albedo in middle latitudes is greatest during the winter season. The amplitude of the seasonal variation of albedo in middle latitudes is greater in the northern hemisphere, however. Ultimately, this must be due to the greater extent of land areas in the northern hemisphere. The relative contributions from cloudiness changes and surface albedo effects to the greater amplitude of the annual variation of mid-latitude albedo in the northern hemisphere have not been quantified, however. The annual variation of zonally averaged albedo has been presented separately for land and ocean areas by *Campbell and Vonder Haar* [1980]. They found that the annual variation of albedo in middle latitudes was largest over land areas in the northern hemisphere. Even over the oceans, however, the annual variation of the albedo was larger in the northern hemisphere than in the southern hemisphere. The reason why the ocean areas in the northern hemisphere should show a larger annual variation in albedo than the ocean areas in the southern hemisphere has not been carefully studied, but it must be related to cloudiness variations associated with land-ocean interactions which have not been fully elucidated.

The seasonal and latitudinal variation in zonally averaged outgoing long-wave radiation is shown in Figure 2*b*. The outgoing long-wave radiation is greatest in the subtropics, dips near the equator, and decreases steadily from the subtropics to the poles. The secondary minimum near the equator is displaced toward the summer hemisphere during the solstitial seasons. This minimum is associated partly with humidity variations [*Warren and Thompson*, 1983] but primarily with the band of tall convective cloud near the equator which is often referred to as the intertropical convergence zone. As we shall see later, however, this cloudiness does not form a zonally uniform band but tends to be most prevalent at the longitudes of South America, Africa, and Indonesia. The major precipitation zones located near these continents tend to move north and south with the sun. Seasonal variations in midlati-

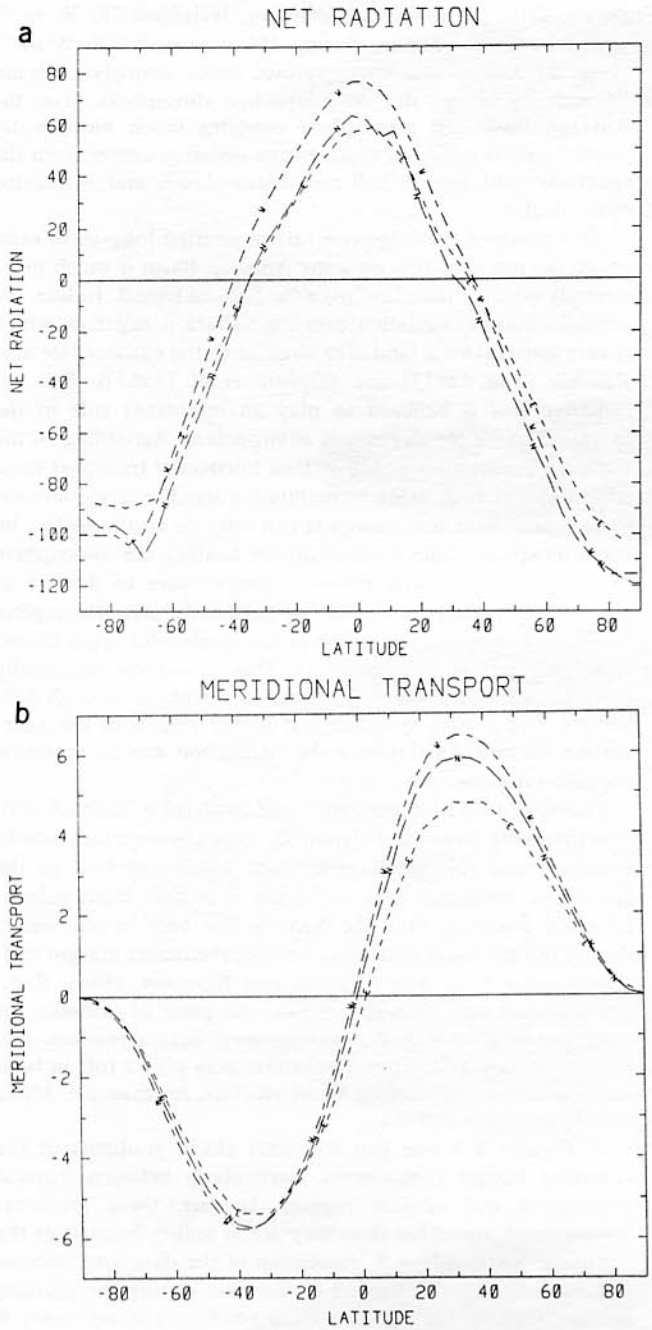

Fig. 3. (*a*) Zonally and annually averaged net radiation from *Ellis and Vonder Haar* [1976] (E), Nimbus 7 ERB WFOV (W), and Nimbus 7 ERB NFOV (N). (*b*) Meridional energy transport implied by the three net radiation curves.

tudes are greater in the northern hemisphere but near the poles are greater in the southern hemisphere.

The net radiation, shown in Figure 2*c*, closely follows the pattern of insolation with positive values around 100 W m^{-2} at the subsolar latitude decreasing to about -160 W m^{-2} near the winter poles. The largest net heating occurs near 30°S near the time of the December solstice.

Meridional Transport

The change in the energy content of an earth-atmosphere column over an integral number of years is small in comparison to the net radiation at the top of the atmosphere. If the earth-atmosphere energy balance (equation (1)) is averaged over an integral number of years, the approximate energy balance equation becomes

$$R = \text{div } \mathbf{T}_A + \text{div } \mathbf{T}_O \tag{6}$$

In words, the net radiation input at the top of the atmosphere must be balanced by the divergence of horizontal transport in the atmosphere and ocean. It is assumed here that nonradiative heating is either small or horizontally invariant. A number of investigators have applied (6) to zonally averaged data. There has been particularly acute interest in using (6) to infer the meridional transport of energy in the ocean as a residual, given estimates of the zonally averaged radiation balance and the poleward transport of energy in the atmosphere [*Vonder Haar and Oort*, 1973; *Oort and Vonder Haar*, 1976; *Hastenrath*, 1982]. It is very valuable to be able to make an indirect estimate of oceanic transport, since measurements of ocean currents and temperature are distributed rather sparsely in space and time so that direct estimates of oceanic heat flux must be assigned a rather large uncertainty. Estimates based on the heat balance of the oceans require that surface fluxes be estimated using empirical formulae. All available methods of estimating oceanic and atmospheric energy fluxes should be pursued vigorously so that independent estimates can be compared.

The total horizontal energy transport in the earth-atmosphere can be estimated with the same accuracy as the net radiation. Net radiation budget measurements at the top of the atmosphere can in principle provide a more accurate estimate of the total horizontal energy transport than any other method. At present, however, net radiation measurements contain rather large uncertainties. The annually and globally averaged net radiation estimates provided by various previous satellite systems vary by approximately 10 W m^{-2}, whereas net radiation is expected to be zero. The latitudinal variation of net radiation for three data sets is shown in Figure 3*a*. There are considerable differences between the three estimates. *Ellis and Vonder Haar*'s [1976] data set has a global mean net radiation of near zero (about $+1$ W m^{-2}); the data set from the Nimbus 7 ERB narrow field of view instrument has a net radiation of about -3 W m^{-2}; and the Nimbus 7 ERB wide field of view data have a globally and annually averaged net radiation of about $+9$ W m^{-2}. If these global mean biases are removed, the annual-mean total meridional energy transport requirement can be estimated from the meridional variation in the net radiation. Figure 3*b* shows the meridional transport requirement inferred from the different data sets. It seems from this comparison that an uncertainty as large as 25% remains in the required poleward energy flux as inferred from radiation budget measurements. The largest differences in this case occur in the northern hemisphere where the transports inferred from the Nimbus 7 data are substantially larger than those inferred from *Ellis and Vonder Haar*'s [1976] data. Similar large variations in the northern hemisphere were found by *Hastenrath* [1982], who included transports inferred from NOAA data [*Gruber*, 1978] and Nimbus 6 ERB data [*Jacobowitz et al.*, 1979]. The Nimbus 6 data also imply much greater poleward transports than any of the earlier data. These larger transports result from a greater equator-to-pole gradient in net radiation. This larger gradient can be seen clearly in Figure 3*a*. The reason for the difference is not known. Instrumentation and data processing have improved with time, so that one might be inclined to favor the estimates from the more recent Nimbus satellites. On the other hand, both the Nimbus 6 and Nimbus 7 satellites were in sun-synchronous noon orbits, whereas the *Ellis and Vonder Haar* [1976] compilation, while based on older data, contains observations from a greater variety of local times. Because of their combination of precise instrumentation, state-of-the-art

processing, and complete diurnal sampling, the ERBE data are expected to narrow the uncertainty in the required equator to pole transport. They may also provide some insight into the reasons behind the differences between the curves in Figure 3.

Geographical Variation

The geographical distributions of seasonal mean radiation budget components estimated from Nimbus 7 ERB narrow field of view data are shown in Figures 4–6. The spatial resolution of the data used to construct these maps is about 450 km, so that a reasonable amount of geographical detail can be seen. In addition to the strong equator-to-pole gradients which have already been noted, a substantial amount of east-west variation associated with the distribution of continents and oceans is apparent. During the December–February (DJF) season the outgoing long-wave radiation is greatest in the subtropical dry zones over the eastern oceans and over the Afro-Asian land desert complex. The long-wave emission has three distinct minima over South America, Africa, and Indonesia. These minima are associated with the presence of deep convective clouds. The albedo is also large in the regions of persistent deep convection. The net radiation in the tropics is greatest over the subtropical oceans. Because of partial compensation between the effects of albedo variations and long-wave variations, the fractional change in net radiation between land and ocean in the tropics is not as large as that of either albedo or emitted long-wave radiation.

In middle and high latitudes of the southern hemisphere the radiation budget components are nearly zonally symmetric. Significant zonal variations in both albedo and long-wave radiation associated with the contrast between land and ocean appear in the northern hemisphere during winter. The long-wave emission is lower over the colder continental areas and higher over the eastern oceans. The albedo is higher over the continents, particularly in those regions where one expects snow cover during the winter.

It is interesting to contrast the summer and winter seasons in the northern extratropics. The contrasts of albedo and long-wave radiation between the continents and the oceans reverse from winter to summer. During the summer the long-wave emission is greater over the continents, and the albedo is greater over the oceans. This is just the opposite of the winter contrast. During the summer the insolation is quite high, and the albedo contrast dominates the effect on net radiation. As a result, at middle and high latitudes there is significantly more net radiative input to the continents than to the oceans during summer. The relatively high albedos over the oceans during summer appear to be associated with the presence of substantial amounts of low cloud.

The components of the radiation budget are closely related to both the surface type and the circulation regime. An interesting illustration of this is found in the contrast between the Sahara Desert during June–August (JJA) and the Amazon basin during DJF. The insolation available and the average solar zenith angle in these two regions during their respective summer seasons are about the same. These two regions also have about the same relatively high planetary albedo, albeit for very different reasons. Few clouds are present over the Sahara, and the high planetary albedo results primarily from the relatively high albedo of the dry, sandy surface. The high albedo over the Amazon basin, in contrast, is associated with the presence of persistent convective cloudiness, and the surface albedo is somewhat lower.

The largest contrast between these two regions can be seen in the outgoing long-wave radiation. Over the Amazon Basin during DJF the long-wave emission is below 230 W m^{-2}, whereas over the Sahara during JJA it exceeds 290 W m^{-2}. Over the Sahara the warm surface emits strongly to space through a relatively dry and cloud-free atmosphere. Over the Amazon Basin the atmosphere contains much more water vapor, and, in addition, much of the emission comes from the relatively cold tops of tall convective clouds and associated cirrus decks.

As a result of the large contrast in emitted long-wave radiation, the net radiation over the Amazon Basin is much more strongly positive than that over the Sahara Desert. In fact, the annual mean net radiation over the Sahara is negative, which is very unusual for a land area so close to the equator (see also *Raschke et al.* [1973] and *Stephens et al.* [1981]). This net radiative loss is believed to play an important role in the maintenance of the dry desert environment. According to (6), if the net radiation is negative, then horizontal transport must supply energy to a region to maintain a steady energy balance. Over a land area this transport can only be accomplished by the atmosphere. One mechanism for heating the atmosphere in a region is for high potential temperature to flow in at altitude, heat adiabatically during subsidence over the region, and then flow out of the region at low levels after being cooled to a lower potential temperature. This circulation continually provides warm dry air to the lower troposphere through subsidence and carries moisture out of the region in the near-surface outflow. In this way the circulation acts to maintain the desert dryness.

Charney [1975] has described and modeled a feedback process involving large-scale dynamics, vegetation-surface albedo coupling, and the radiation balance which can lead to the growth or shrinkage of desert areas. It is clear from paleontological evidence that the Sahara has been much wetter during the past and that movement of the desert margin continues today [e.g., *Street-Perrott and Harrison*, 1984]. Radiation budget data provide an essential piece of evidence for understanding the linkages between large-scale dynamics, surface hydrology, and net radiation that may play a role in both regional and global climate sensitivity (see, for example, *Mintz* [1984] and *Rasool* [1984]).

In Figures 4–6 one can see fairly sharp gradients in the radiation budget components, particularly between tropical continental and oceanic regions. In fact, these gradients appear much smoother than they are in reality because of the relatively coarse 4.5° × 5° resolution of the data and because some smoothing was applied to the data during the plotting process. Clearly, very good spatial resolution is necessary if one expects to unambiguously separate land and ocean regions. Observations from the scanner instruments on the ERBE satellites will be used to produce daily and monthly average maps at 2.5° × 2.5° resolution for use in studies requiring good spatial resolution.

Diurnal Variations

The earth radiation budget components vary systematically with the local time at a fixed point. Albedo and absorbed radiation vary over the daylight hours as a result of the natural dependence of the scattering on solar zenith angle and because the atmospheric state, particularly the amount and type of cloud, may vary systematically with local time. Outgoing long-wave radiation varies throughout the day as a result of diurnal variations in cloudiness, surface temperature, atmospheric temperature, and humidity. Recently, the excellent temporal and spatial resolution provided by geosynchronous satellite data has been exploited to study regional diurnal vari-

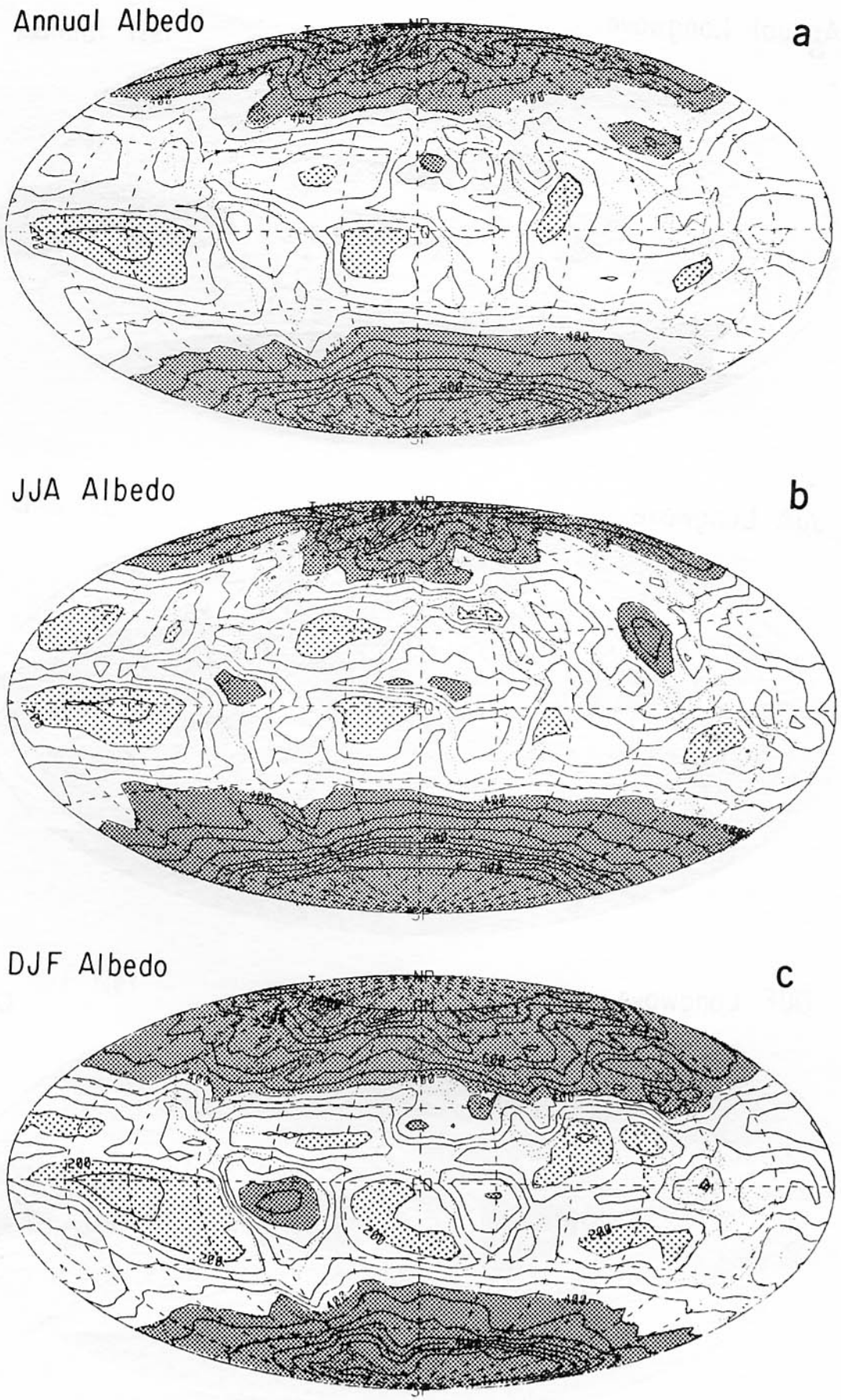

Fig. 4. Albedo derived from the Nimbus 7 ERB NFOV instrument in Hammer equal-area projection for (*a*) the annual average from June 1979 through May 1980, (*b*) the average for June, July, and August (JJA) 1979, and (*c*) the average for December 1979 and January and February 1980 (DJF). Contour interval is 0.05. Areas with albedos greater than 0.40 have a dense dot pattern. Areas with albedos lower than 0.20 have a sparse dot pattern.

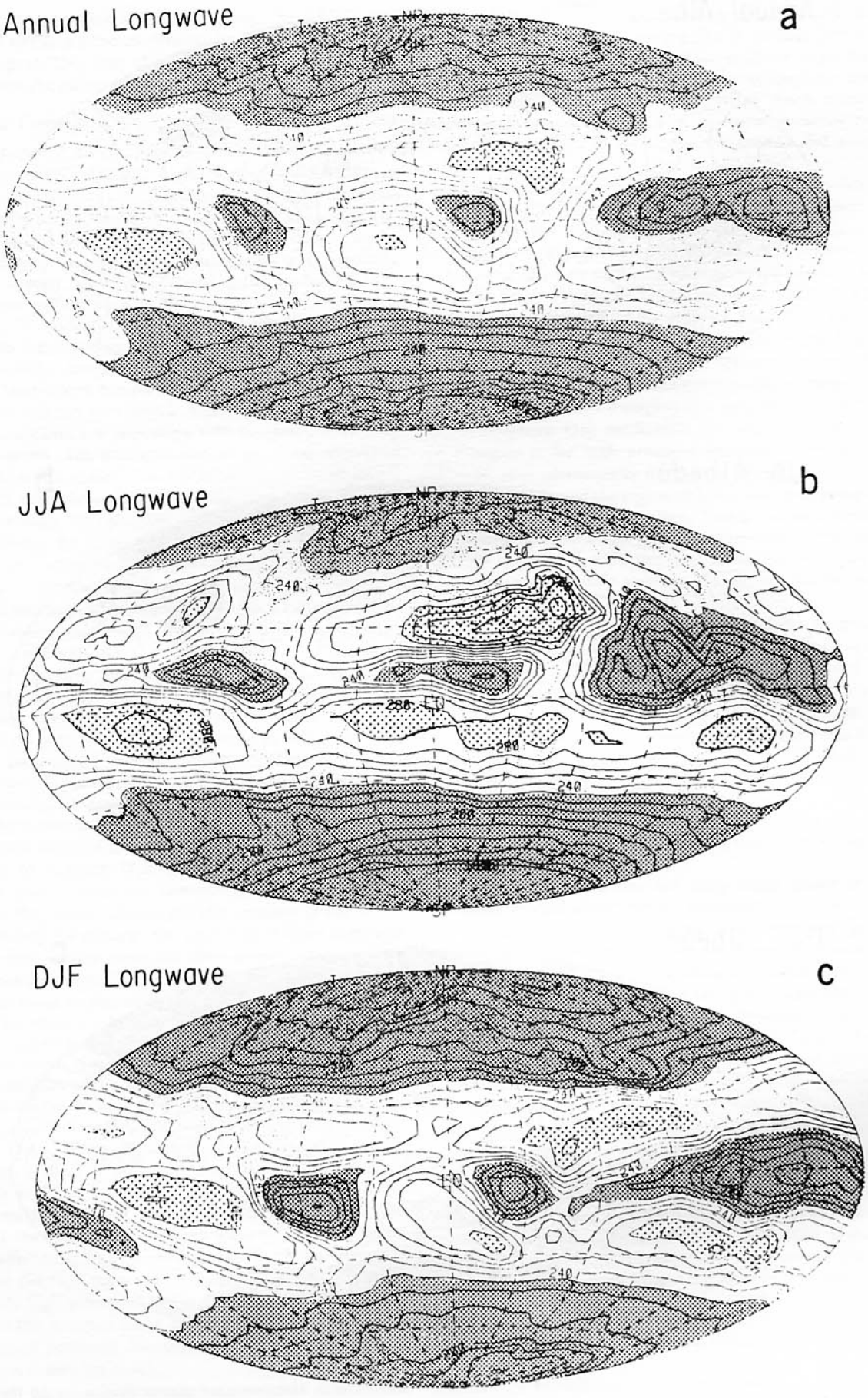

Fig. 5. Same as Figure 4 except for outgoing long-wave radiation in watts per meter squared. Contour interval is 10 W m^{-2}. Areas with outgoing long-wave radiation less than 230 W m^{-2} have a dense dot pattern. Areas with values greater than 280 W m^{-2} have a sparse dot pattern.

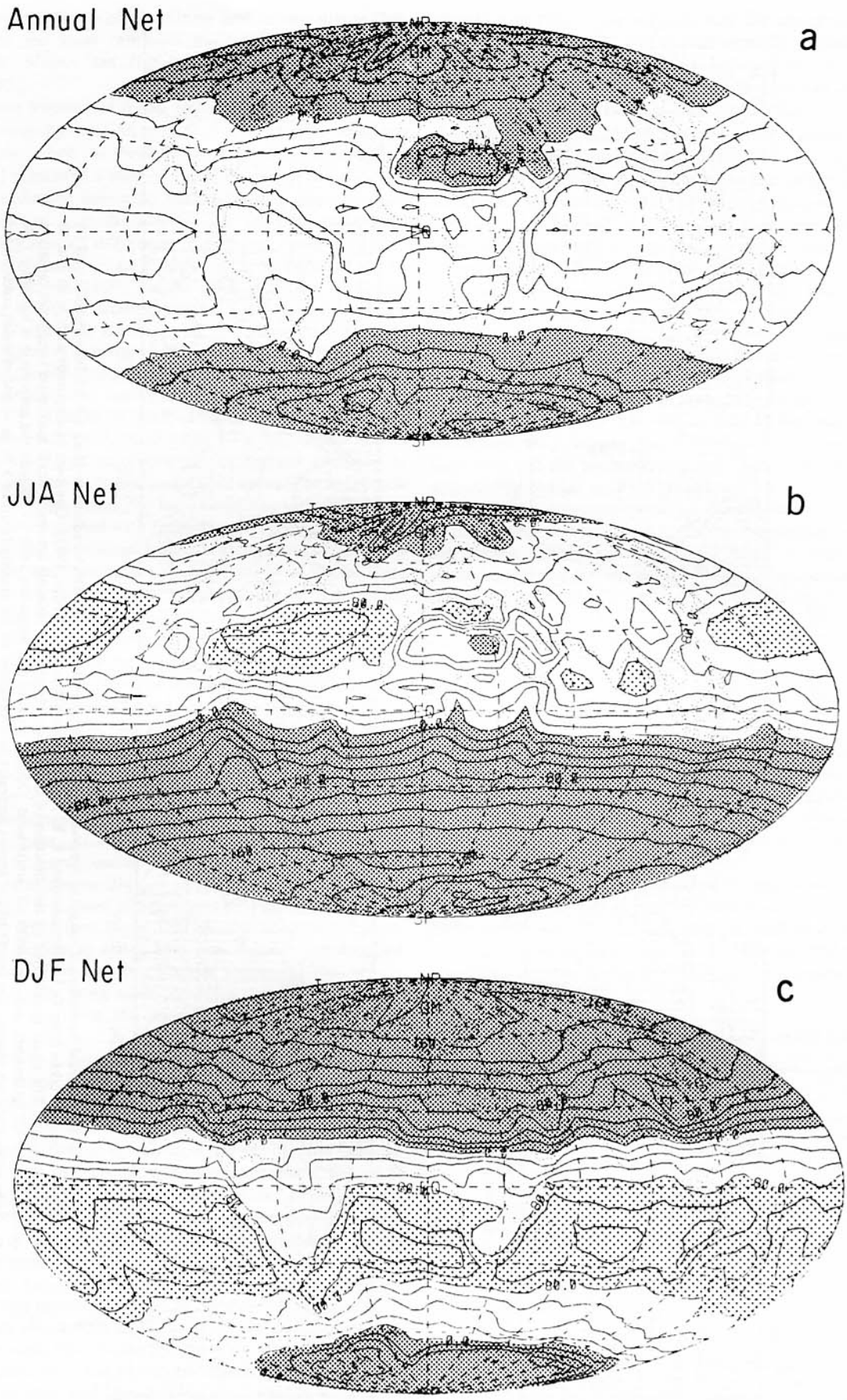

Fig. 6. Same as Figure 4 except for net radiation in watts per meter squared. Contour interval is 20 W m^{-2}. Areas with negative net radiation have a dense dot pattern. Areas with positive net radiation greater than 80 W m^{-2} have a sparse dot pattern.

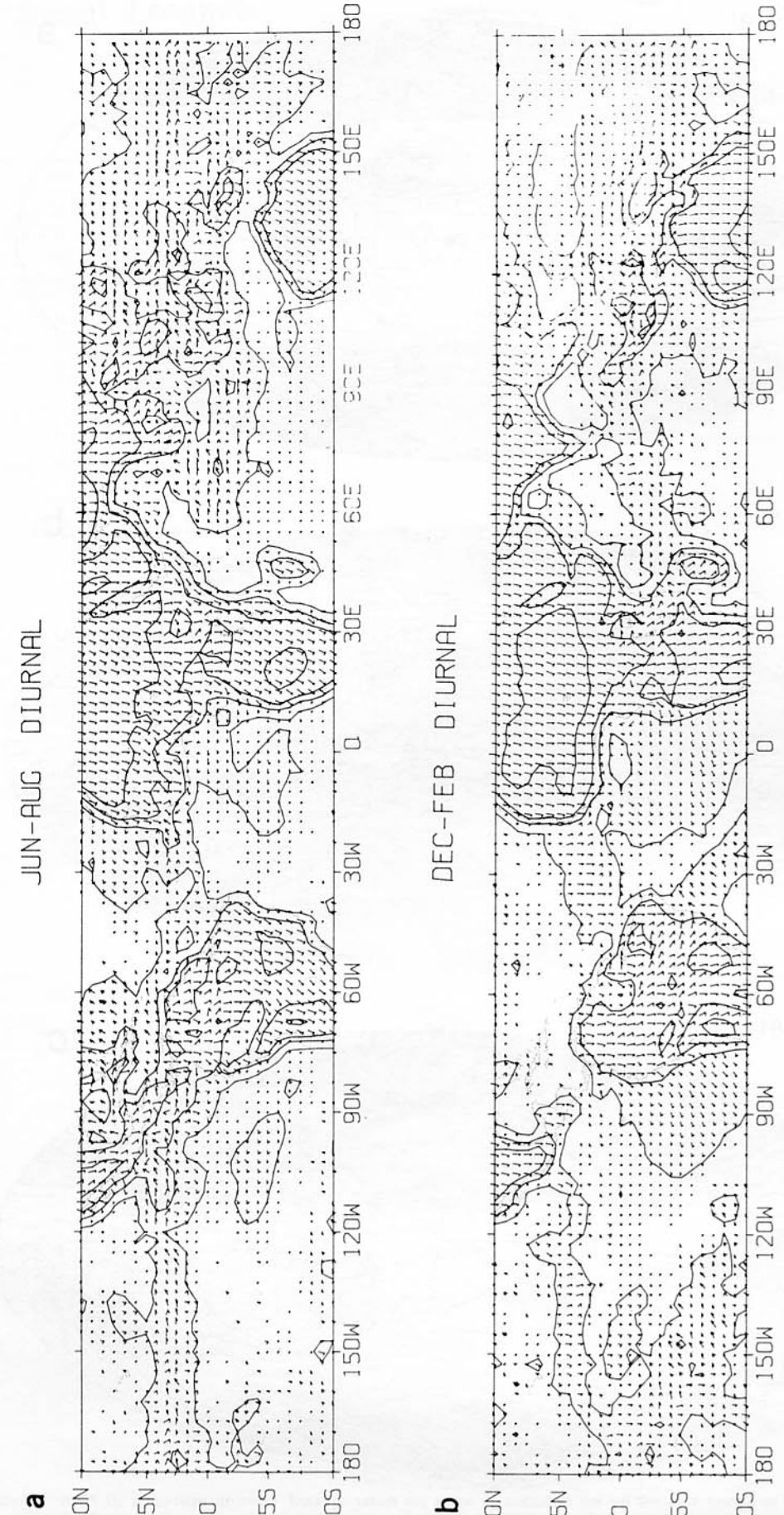

Fig. 7. The first diurnal harmonic of outgoing long-wave radiation estimated from NOAA radiometer data for (*a*) June–August and (*b*) December–February (taken from D. L. Hartmann and E. E. Recker (unpublished manuscript, 1985)). Contours of amplitude at 2, 5, 10, and 20 W m^{-2} are shown. The phase is indicated by the direction of the arrows. Northward pointing arrows indicate maximum long-wave radiation occurs at 0000 LT (midnight), eastward 0600 LT, southward 1200 LT (noon), and westward 1800 LT. Where the amplitude is less than 1 W m^{-2}, the arrows are not shown. The length of the arrows increases in proportion to the amplitude up to 5 W m^{-2} and remains constant for amplitudes greater than 5 W m^{-2}.

ations in temperature and cloudiness and to investigate their influence on the local radiation budget [e.g., *England and Hunt*, 1984; *Minnis and Harrison*, 1984*a*, *b*, *c*; *Duvel and Kandel*, 1985].

It has been known for many years that large diurnal variations in outgoing long-wave radiation exist over relatively dry land areas when the insolation is large. *Raschke and Bandeen* [1970] presented a map of the difference in the outgoing long-wave radiation measured near noon and near midnight by the Nimbus 2 medium-resolution infrared radiometer (MRIR). They showed differences of 40 W m^{-2} and more over extensive continental areas. Similar features were shown by *Short and Wallace* [1980] for the 0900–2100 LT difference map for the NOAA 4 satellite. Figure 7 shows the amplitude and phase of the first harmonic of the diurnal variation in outgoing long-wave radiation inferred by D. L. Hartmann and E. E. Recker (unpublished manuscript, 1985) from NOAA satellites in four different sun-synchronous orbits (NOAA 2–5, 0900–2100 LT; TIROS N, 0330–1530 LT; NOAA 6, 0730–1930 LT; and NOAA 7, 0230–1430 LT). This figure shows very clearly the large amplitude of the diurnal variation in long-wave radiation over the major land areas. The amplitude is particularly large where the land surface is very dry. These variations are associated with large diurnal changes in surface temperature. The maximum long-wave emission occurs near noon or in the early afternoon. Also of interest in Figure 7 are regions over the oceans where the amplitude of the diurnal harmonic is smaller than over the land but is still significant, and where the phase shows a very consistent behavior over rather large areas. Over the regions where we know oceanic stratus cloud predominates, for example, the outgoing long-wave radiation peaks consistently in the midafternoon. Such regions are apparent in the subtropics to the west of most continents, especially in the summer hemisphere. The best developed of these are those to the west of South America and Africa during the December–February season. These variations are consistent with the observed diurnal variation in stratus cloudiness. *Minnis and Harrison* [1984*a*, *b*] used GOES-East observations of visible albedo and long-wave emission to estimate the diurnal variations of cloud coverage. In the stratus region west of South America during the month of November 1978 they found that the fractional area coverage by cloud peaked at about 85% near sunrise and dropped to a minimum of about 50% around sundown. This would suggest maximum long-wave emission around sundown, which is consistent with the phase of the diurnal harmonic shown in Figure 7.

Large diurnal variations in long-wave radiation also occur over the wet tropical continental areas such as the Amazon and Congo (Zaire) river basins. The amplitudes are generally smaller than over dry continental areas, however, because diunal surface temperature variations are smaller and because diurnal variations in deep convection are prevalent. Figure 8, taken from the work by *Minnis and Harrison* [1984*c*], shows the diurnal variation of cloud cover and the corresponding diurnal variations in the radiation budget parameters during the daylight hours over the southeast Pacific stratus region and over the Amazon Basin. In the oceanic stratus region (21.4°S, 86.3°W) the cloud coverage decreases from near 90% at 0600 LT to about 50% in the early afternoon and remains there until sunset. This causes the morning albedos to be significantly higher than the afternoon albedos. The long-wave emissions from clear and cloudy areas each remain fairly constant over the course of the day with the clear-sky emission 15–20 W m^{-2} higher. The constancy of the emission from the cloudy and clear areas suggests that the temperatures of the surface, air, and cloud top are all remaining constant. A significant diurnal variation in total emission results solely from the diurnal change in the fractional area coverage of cloud.

In contrast, over the Amazon Basin (10.1°S, 55.1°W) the diurnal variation in cloud amount is only about 10% with higher values near sunrise and sunset. The clear-sky emission varies by about 10 W m^{-2} with the largest values in the early afternoon. A small clear-sky emission variation is expected, because solar heating of the surface is strongly buffered by evaporation so that the resulting surface temperature variations are small. A very large 40 W m^{-2} diurnal variation in the long-wave flux from cloudy skies exists, however, which appears to dominate the total diurnal variation. The diurnal variation of the long-wave radiation over the highly convective Amazon Basin appears to result primarily from a diurnal variation in the average altitude of the cloud tops rather than from variations in either cloud amount or surface temperature. Maximum long-wave emission occurs in the morning when cloud tops are relatively low and warm. After noon the cloud tops rise, and the long-wave emission decreases without any appreciable change in cloud amount.

Significant consistent diurnal variations also appear in Figure 7 near the regions where deep convection occurs over the oceans. Amplitudes exceeding 2 W m^{-2} occur just north of the equator in the vicinity of the Intertropical Convergence Zone (ITCZ), in the region of the South Pacific Convergence Zone (SPCZ) extending southeastward from the equatorial dateline, and, during the December–February season, in the region of the South Atlantic Convergence Zone extending southeastward from the vicinity of Rio de Janiero. The phase of the diurnal variation in the ITCZ is different during December–February than it is during the June–August season. During the northern hemisphere summer, when the ITCZ is better developed, the maximum long-wave emission occurs in the early morning. During the December–February season, however, the maximum long-wave emission occurs at noon. This phase shift between the seasons occurs over both the Pacific and Atlantic oceans.

Two features of the diurnal cycle in long-wave emission in the vicinity of the ITCZ over the oceans require explanation. These are the fact that the amplitude is small and the fact that the phase shift between seasons is dramatic but consistent over large areas in two oceans. Both of these observations can

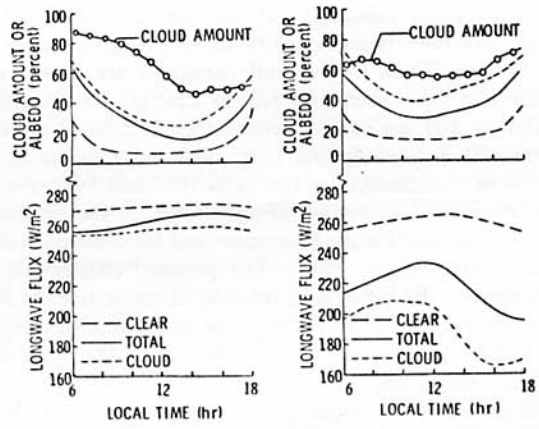

(a) Pacific Sc, lat. = 21.4°S, long. = 86.3°W

(b) Deep convection, lat. = 10.1°S, long. = 55.1°W

Fig. 8. Mean hourly, daytime, and regional cloud amounts and radiative parameters for November 1978, taken from the work by *Minnis and Harrison* [1984*c*].

be explained by the apparent fact that the phase in the diurnal variation in cloud amount in these regions depends on the altitude of the cloud top. *Albright et al.* [1984] show convincing evidence that over the Pacific ITCZ during northern hemisphere winter, clouds with tops between 273 K (600 mbar) and 253 K (400 mbar) have a diurnal variation in fractional area coverage with maximum coverage occurring near midnight. This would tend to give a noon maximum in outgoing IR. Clouds with tops colder than 243 K (above 300 mbar) show a maximum fractional area coverage around 0900 LT. The diurnal variation in these high clouds would act to reduce the noon maximum in the outgoing long-wave radiation associated with the middle level cloud.

Over the SPCZ, *Albright et al.* [1984] again find a noon minimum in middle level cloud (273–253 K; 600–400 mbar). This minimum occurs earlier in the day for higher, colder clouds so that for cloud tops at 223 K (200 mbar), minimum coverage occurs in the early morning and a sharp maximum occurs in midafternoon. It is apparently this upper level cloud variation which dominates the outgoing long-wave variation and causes maximum long-wave emission to occur in the morning over the SPCZ.

The work of *Albright et al.* [1984] suggests very strongly that in regions of deep convection over the oceans the type of cloud present may vary more substantially during the day than does either the amount of cloud or the outgoing long-wave radiation at the top of the atmosphere. Theoretical calculations have shown that cloud geometry has important effects on transfer of both solar radiation [e.g., *McKee and Cox*, 1974; *Davies*, 1978] and long-wave radiation [e.g., *Harshvardan et al.*, 1981; *Ellingson*, 1982; *Duvel and Kandel*, 1984]. It is possible that the changing cloud geometry over the course of the daylight hours may have an important influence on both the diurnal mean albedo and the long-wave emission. The full diurnal coverage available from the ERBE instruments on the Earth Radiation Budget Satellite (ERBS) will allow the study of these problems.

Interannual Variations

A decade-long record of radiation budget data inferred from narrow-band radiometers on NOAA satellites is currently available [*Gruber and Winston*, 1978; *Gruber and Krueger*, 1984]. Despite changes in satellites and local observing time during this period, the data are useful for studies of interannual variability [*Short and Cahalan*, 1983; *England and Hunt*, 1984]. Monthly, seasonal, and even annual mean radiation budget components have exhibited very large changes from year to year. These interannual variations are largest in the tropics and are closely related to changes in atmospheric circulation and sea surface temperature. Regional anomalies in seasonal mean outgoing long-wave radiation as large as ± 50 W m^{-2} accompanied the 1976–1977 and 1982–1983 episodes of warm sea surface temperatures in the central and eastern equatorial Pacific [*Liebmann and Hartmann*, 1982; *Rasmusson and Wallace*, 1983]. The primary change during a warm episode (El Niño) is an increase in convective cloudiness in the central Pacific and a decrease in convective cloudiness near Indonesia [*Heddinghaus and Krueger*, 1981; *Weickmann*, 1983; *Lau and Chan*, 1983].

The anomalies in outgoing long-wave radiation can be used to characterize the total diabatic heating in the tropics. When outgoing long-wave radiation is anomalously low, deep convective clouds are present, and the latent heat exchange and radiative changes associated with their presence give rise to a net heating of the atmosphere. This heating drives large-scale circulations which produce the moisture flux necessary to sustain the convective clouds. Horizontal distributions of heating inferred from outgoing long-wave data have been used to force linear models of both the mean seasonal wind patterns [*Hartmann et al.*, 1984] and wind pattern anomalies associated with warm events in the Pacific [*Gill and Rasmusson*, 1983].

The large changes in top-of-atmosphere albedo and long-wave emission associated with warm events undoubtedly result in large local changes in the surface radiative heating. Because of the large thermal capacity of the ocean, the limited area extent of the anomalies, and the fact that anomalies of opposite sign tend to occur in association with each other, it is questionable whether anomalies entirely over the ocean lead to any substantial change in the global mean radiation budget. It is possible that only the spatial distribution of radiative heating changes significantly and that this is compensated for by horizontal transport of the large-scale flow field. Interannual variations in the distribution of convection between land and ocean are much more important because of the need for fresh water on land and may also have a measurable impact on the planetary radiation budget [*Hartmann*, 1984]. Study of the relationship of regional anomalies in radiation budget components to the global mean radiation balance is only beginning. Recently, increasing attention has been given to the close relationship between anomalies in outgoing long-wave radiation and anomalies in global circulation patterns [*Murakami*, 1980; *Weickmann*, 1983; *Lau and Chan*, 1983; *Liebmann and Hartmann*, 1984]. These studies have shown very clearly that anomalies in radiation budget components are associated with anomalies in the large-scale wind patterns. While the most spectacular radiation budget anomalies seem to occur in the tropics, anomalies have also been observed in the polar regions (S. Charlambides et al., unpublished manuscript, 1984). Studies of the effect on climate and weather prediction of the coupling between atmosphere dynamics and the radiation budget are under way at many institutions.

3. OBSERVATIONAL STUDIES OF CLOUD FORCING AND FEEDBACK

Introduction

One of the goals of climate research is to understand the maintenance of the current climate well enough so that the response of the climate to a given change in parameters can be predicted with confidence. The parameters of interest include such things as atmospheric CO_2 concentration, aerosol loading, solar flux, and surface albedo. One of the major remaining uncertainties in the evaluation of the sensitivity of the earth's climate is the role of clouds. The primary effects of clouds of water droplets and ice are to absorb and emit terrestrial radiation and scatter solar radiation. Because of the decrease of temperature with height in the atmosphere, clouds decrease the terrestrial radiation emitted to space. This decrease would contribute to an increase in the net radiation at the top of the atmosphere. The scattering of solar radiation by clouds increases the planetary albedo under most circumstances, however. This higher albedo leads to a decrease in the net radiation at the top of the atmosphere. The effects of clouds on emitted long-wave and absorbed solar radiation both are potentially large and have opposing influences on the net radiation [*Schneider*, 1972]. An accurate evaluation of the effect of cloudiness on the net radiation balance is thus itself a delicate matter of resolving a residual between two much larger terms. Nonetheless, the evaluation of the effect of the current distri-

bution of cloudiness on the top of the atmosphere radiation balance is straightforward in principle. The problems have arisen primarily at the practical level in obtaining adequate data and in choosing the best analysis procedure. The attempts that have so far been made to evaluate the effect of cloudiness on the net radiation will be reviewed here. The even more interesting question of how the cloudiness distribution responds to a change in climate is difficult to address squarely in an observational study. This question will be discussed later in the section on theory and modeling. The simple direct effect of the current distribution of cloud on net radiation may be termed the "cloud forcing" problem. Potential changes in the cloud distribution associated with a climate change and the influence of these changes in cloudiness on climate sensitivity may be referred to as the "cloud feedback" problem.

Conceptual Framework

In order to develop a useful conceptual framework for sensitivity studies, it is usually assumed that the radiation budget components can be expressed in terms of a very small number of variables. The dependence of the model climate on each variable can then be expressed very compactly in terms of derivatives. This approach was introduced initially for expressing the sensitivity of energy balance climate models where, in fact, the only independent variable is often surface temperature. In equilibrium the globally and annually averaged net radiation must be zero, so that from (3) and (5) we must have

$$F = S = S_0(1 - \alpha_p) \tag{7}$$

Here F and α_p are assumed to depend only on the surface temperature T_s, and S_0 is assumed to be an external parameter. *Schneider and Mass* [1975] suggested the sensitivity parameter

$$\beta = S_0 \frac{dTs}{dS_0} \tag{8}$$

which is a measure of the sensitivity of the global mean surface temperature to variations in the global mean solar flux density S_0. The derivative is assumed to be evaluated for the equilibrium climate. By differentiating (7) with respect to T_s, using (5), and rearranging, the sensitivity parameter (8) can be expressed as

$$\beta = S_0 \frac{dT_s}{dS_0} = \frac{F}{S_0(d\alpha_p/dT_s) + (dF/dT_s)} = \frac{+F}{-dR/dT_s} = \frac{S}{-dR/dT_s} \tag{9}$$

The sensitivity parameter β is then just equal to the magnitude of the absorbed solar or emitted terrestrial radiation, which must equal each other in equilibrium, divided by the rate at which their difference, the net radiation R, changes with global mean surface temperature, which has been assumed to uniquely define the climate. The terms in (9) can usually be evaluated rather easily for energy balance climate models, since relatively few variables are generally allowed to vary. The complexity involved in applying (9) to observations or complex models can easily be imagined by noting that in general,

$$\frac{dR}{dT_s} = \frac{\partial R}{\partial T_s} + \sum_{i=1}^{N} \frac{\partial R}{\partial x_i} \frac{dx_i}{dT_s} \tag{10}$$

where x_i is the list of variables that can influence the net radiation, such as the characteristics of the cloud distribution, humidity distribution, lapse rate, and surface albedo. It is clear that in general, N is not a small number. In order for (9) and (10) to be a useful simplification of the climate sensitivity problem it must be assumed that the net radiation can be expressed approximately in terms of a few variables. The variables which have most often been considered and which seem most important are absolute humidity $\mathbf{q}$, surface albedo α_s, and fractional area coverage of cloudiness C. *Manabe and Wetherald* [1967] have argued that to first order, humidity variations can be taken into account by assuming constant relative humidity rather than constant absolute humidity. The resulting increase of atmospheric water vapor with increasing temperature reduces the rate at which outgoing long-wave radiation increases with temperature. This positive coupling between atmospheric temperature and long-wave opacity increases the sensitivity parameter β over what it would be in the case of constant absolute humidity by about a factor of 2. Surface albedo changes associated with snow and ice have long been considered to be an important contributor to the sensitivity of climate, particularly on glacial time scales. Surface albedo variations associated with changes in vegetation may also play a significant role in climate change.

While much further work needs to be done to clarify the role of humidity and surface albedo variations, the question of the role of cloudiness in climate sensitivity will be emphasized here to illustrate the role of radiation budget measurements in sensitivity studies. For the sake of argument one can assume that the only variables that affect net radiation R are the surface temperature T_s and the fractional area coverage of cloudiness, C. In this case, (10) becomes

$$\frac{dR}{dT_s} = \frac{\partial R}{\partial T_s} + \frac{\partial R}{\partial C} \frac{dC}{dT_s} \tag{11}$$

where again it has been assumed that the climate, including the cloudiness, is uniquely related to the global mean surface temperature. The relation (11) expresses mathematically the hypothesis that the sensitivity of the net radiation to climate change consists of two parts: (1) the result of the temperature change by itself and (2) the result of the cloudiness changes associated with the temperature change. The latter is in turn the product of two terms. The first term is the partial derivative of the net radiation with respect to cloud cover (cloud forcing), and the second is the total change in cloud cover resulting from a given global temperature change. The first term can be written as

$$\frac{\partial R}{\partial C} = -S_0 \frac{\partial \alpha}{\partial C} - \frac{\partial F}{\partial C} \tag{12}$$

As mentioned earlier, it is expected that increasing cloud cover will usually increase the planetary albedo α and decrease the outgoing long-wave radiation F so that the two terms on the right in (12) will be of opposite sign. The relative magnitudes of these two terms can be estimated using observations of the radiation budget.

It is important to remember that (11) and (12) explicitly assume that net radiation is a function only of the total cloud coverage and the surface temperature. In reality, planetary albedo and outgoing long-wave radiation depend strongly on the type of cloud, its shape, and vertical distribution. In applying (11) and (12) one must assume that the cloud type remains fixed and that only changes in cloud amount occur. In determining the sensitivity of climate, changes in cloud type may easily be as important as changes in total cloud amount. In fact, the cloud feedback effect may very well depend on the mechanism whereby the global temperature is altered and

how this affects the cloud type and amount. When attempting to estimate the terms in (12) using observations, it is never possible to assure that all other variables remain fixed and that only the total cloud amount varies. The manner in which extraneous variables influence estimates of $\partial R/\partial C$ will depend on the data and type of variation used to approximate the partial derivative. For example, latitudinal variations, longitudinal variations, daily variations, seasonal variations, and interannual variations can each be used to estimate $\partial R/\partial C$, but the interpretation of the result is different in each case. Some studies of this type are reviewed in the next section.

Investigations of Cloud Forcing and Cloud Feedback

Cess [1976] has attempted to infer $\partial R/\partial C$ and dR/dT_s from latitudinal climate change. He used zonally and annually averaged radiation budget data from *Ellis and Vonder Haar* [1976], together with cloudiness data from *London* [1957] and *van Loon* [1972] and climatological surface temperatures. These data were available for eighteen 10°-wide latitude belts. Multiple regression was performed to determine a linear predictor for the outgoing long-wave radiation in terms of surface temperature and cloud cover. Cess found that in both hemispheres the dependence could be expressed to good approximation as

$$F = 257 + 1.6T_s - 91C \tag{13}$$

The planetary albedo α_p is often expressed as a combination of a clear-sky albedo α_s and a cloudy-sky albedo α_c:

$$\alpha_p = \alpha_c C + \alpha_s(1 - C) \tag{14}$$

From (14) one can easily obtain

$$\frac{\partial \alpha_p}{\partial C} = \alpha_c - \alpha_s \tag{15}$$

Cess [1976] obtained measurements of α_p and α_s and estimated α_c as a residual in (14). The latitudinal variation of the cloud albedo determined in this manner is consistent between the two hemispheres and with cloud albedos estimated in other ways. Substituting (13) and (15) and (12) and using $\alpha_c = 0.44$ and $\alpha_s = 0.18$, Cess obtained

$$\frac{\partial R}{\partial C} = -S_0 \frac{\partial \alpha_p}{\partial C} - \frac{\partial F}{\partial C} = -88.4 + 91 = 2.6 \text{ W m}^{-2} \tag{16}$$

Thus the effect of cloudiness changes on the net radiation was found to be very small in comparison to the individual effects on absorbed solar and emitted long-wave radiation which were approximately equal in magnitude and opposite in sign.

Before continuing, it is important to point out an important distinction between the work of *Cess* [1976] and the works described below. Cess used latitudinal variations in annually and zonally averaged quantities as an approximation to climate change in an attempt to estimate the effect of cloud feedback on the sensitivity of climate. Changes in cloud type, which are certainly manifest as one moves from equator to pole, are thus included as part of the cloud-climate feedback process. Whether latitudinal or seasonal variations are appropriate analogs for climate change can be questioned [e.g., *Hartmann and Short*, 1980], but in fact, attractive alternatives for observational studies are not available.

The studies mentioned below either explicitly or implicitly employ differences between clear and cloudy skies in a particular region during a particular season. Therefore no implication of climate change is involved. These studies indicate how clouds influence the regional mean energy budgets of the present climate. The sensitivity of the current radiation budget to current cloudiness inferred from these studies should not be confused with the effect of cloud feedback on the radiation budget during a climate change inferred by Cess.

Ellis [1978] used instantaneous measurements from the medium-resolution infrared radiometer (MRIR) on Nimbus 3 to develop a clear-sky climatology. The clear-sky albedo was determined to be the minimum value observed in a particular area during a 7-day period. The cloud-free long-wave emission was assumed to be the maximum value observed during the same period of time. In this way a seasonal and zonal average clear-sky climatology was built up. In order to determine the effect of clouds on the net radiation, Ellis used the following approximation:

$$\frac{\partial R}{\partial C} = \frac{R_{\text{average}} - R_{\text{clear}}}{C} \tag{17}$$

where R_{average} is the net radiation averaged over all data, R_{clear} is the average of the clear-sky data, and C is the average cloud coverage. This method directly compares the net radiation of clear skies and average conditions at a particular latitude and season. In (17) the numerator is the radiative forcing by clouds, and the term $\partial R/\partial C$ is a measure of the sensitivity of net radiation to changes in the cloud amount. Ellis found that the effect of clouds on the absorbed solar radiation was about twice as large as their effect on emitted long-wave radiation. His estimate of $\partial R/\partial C = -37$ W m^{-2} suggests that the current distribution of cloudiness substantially reduces the global mean net radiation. Ellis also evaluated the individual contributions of solar and terrestrial radiation to the net forcing:

$$\frac{\partial R}{\partial C} = -S_0 \frac{\partial \alpha_p}{\partial C} - \frac{\partial F}{\partial C} = -79 + 42 = -37 \text{ W m}^{-2} \tag{18}$$

Interestingly, comparison of (18) with (16) reveals that the sensitivity of albedo to cloudiness estimated by Ellis agrees with the corresponding term estimated by *Cess* [1976] but that their estimates of the effect of cloudiness on long-wave emission differ substantially. This difference is not necessarily cause for concern, since the quantities inferred in the two studies must be interpreted differently.

Ohring and Clapp [1980] and *Ohring et al.* [1981] used monthly mean NOAA scanning radiometer (SR) data at specific points to estimate $\partial R/\partial C$. Their results were in general agreement with those of *Ellis* [1978], particularly in regard to the smaller estimate obtained for $\partial F/\partial C$.

Hartmann and Short [1980] used daily observations of the radiation budget from the NOAA SR data set to estimate the relative magnitudes of the effects of clouds on solar and terrestrial radiation. To do this, they used the following relationship:

$$\frac{\partial R}{\partial C} = \frac{\partial F}{\partial C}\frac{\partial R}{\partial F} = -\frac{\partial F}{\partial C}\left[S_o \frac{\partial \alpha_p}{\partial F} + 1\right] \tag{19}$$

The quantity in brackets is a dimensionless number which measures the relative magnitude of the effect of cloud on absorbed solar and outgoing terrestrial radiation. The partial derivative inside the brackets is assumed to represent the ratio of the changes in albedo and outgoing terrestrial radiation resulting from a change in cloud amount. This partial derivative was estimated by regression on daily observations at a point. The results of *Hartmann and Short* [1980] were in agreement with those of *Ellis* [1978] and *Ohring and Clapp*

[1980] on the essential point that the effect of clouds on solar radiation was substantially larger than the long-wave effect, so that the result of an increase in cloud amount would be a reduction in net radiation.

The estimates of cloud effects by *Hartmann and Short* [1980] and *Ohring et al.* [1981] were presented in map form so that the geographical variability resulting from different cloud types and surface conditions could be seen. These maps emphasize very strongly the important effect of oceanic stratus clouds on the net radiation balance. Because of their high albedos as compared to the ocean and their low altitude and consequently warm tops, stratus clouds greatly decrease the absorbed solar radiation while affecting the outgoing terrestrial radiation very little. Low stratus clouds cover large areas of the tropical oceans and are also prevalent over the middle- and high-latitude oceans during summer.

Improved Observational Studies of Cloud Forcing

All previous estimates of the effect of cloudiness on the radiation balance suffer from one or more obvious problems. The major problems are three: (1) the scene is not adequately known; (2) the diurnal cycle is not properly sampled; and (3) the frequencies of radiation sampled do not include the complete emission bands of the sun and earth. These problems will be discussed in turn below.

In all of the studies described above, changes in the radiation budget components were assumed to result exclusively from changes in a small subset of those variables which can influence the net radiation. Most often, only the fractional area coverage of cloudiness is assumed to vary, although sometimes surface temperature is also included. Solar zenith angle effects on albedo must be modeled in some way to account for diurnal, seasonal, and latitudinal variations, if they are present.

Variations in cloud type are never taken into account, since reliable data are not available. Humidity and temperature variations which may be correlated with cloudiness are also routinely ignored. Neglect of such factors as cloud type, humidity, and temperature variations can lead to problems in interpreting changes in radiation budget components. *Cess and Ramanathan* [1978] have discussed the effect of varying cloud type on estimates of the sensitivity of long-wave emission to cloudiness.

The seasonal variations in cloud type can be as significant as the change in cloud amount. In the tropics the penetrative cumulonimbus cloud and associated cirrus tend to move north and south seasonally. When they are absent, nonpenetrative cumulus and stratocumulus are present. A change in cloud type from stratocumulus to cumulonimbus, as may occur seasonally in the tropics, would be associated with a large decrease in outgoing long-wave but a comparatively small change in absorbed solar radiation. Ignoring cloud type changes in this case would then result in an underestimate of the solar effect relative to a large long-wave effect.

If daily variations are used to estimate cloud forcing, the effect of changing cloud type can be reduced by choosing regions and times for which the cloud population is expected to remain constant. In this case, however, changes in temperature and humidity that occur in association with changes in cloud amount could color the result. Many of the uncertainties associated with not knowing exactly what is causing the changes in the radiation budget components will be reduced during ERBE. The scanner data will be used to produce a crude but potentially useful scene identification. In addition, the ERBE operational period overlaps that of the International Satellite Cloud Climatology Project (ISCCP). ISCCP will provide a monthly cloud climatology as well as a collection of raw satellite data that will be capable of characterizing the cloud field. The ERBE project itself will collect auxiliary data for use in validating the scene identification.

No currently available estimate of the radiation budget is based on data which adequately sample the diurnal variation. These data are potentially biased because of imperfect modeling of zenith angle effects or inadequate sampling of real diurnal variations in temperature, humidity, cloud amount, and cloud type. Because of the more complete sampling of all local times anticipated from ERBS in conjunction with NOAA-F and NOAA-G, the ERBE data will allow diurnal variations to be explicitly measured.

Because of the necessity of separating reflected solar radiation from emitted terrestrial radiation, all radiation budget instruments must employ frequency filters. Instruments designed specifically to measure the radiation budget are usually provided with filters which have as sharp a cutoff as possible between solar and terrestrial wavelengths and uniform transmission within the entire solar and terrestrial bands. It is possible, however, to infer broadband radiative fluxes from measurements in narrow spectral bands [e.g., *Gube*, 1982]. This is done in the case of the NOAA SR data, where broadband fluxes are inferred from measurements in the visible band (about 0.5–0.7 μm) and in the 11-μm window region (10.5–12.5 μm) [*Gruber and Winston*, 1978]. While regressions from narrow-band measurements can characterize the broadband fluxes very well, estimates of broadband fluxes based on narrow-band and observations are inappropriate for studies where the wavelength dependence of absorption or scattering is important. Studies of cloud forcing of the net radiation fall into this category.

Cess et al. [1982] compared estimates of cloud forcing based upon seasonal variations in the tropics from two broadband data sets and the NOAA SR narrow-band estimates. The two broadband data sets [*Ellis and Vonder Haar*, 1976; *Campbell and Vonder Haar*, 1980] produced similar results, and both suggested that the long-wave effect was slightly larger than the solar effect. In sharp contrast the NOAA SR data, when analyzed in the same way, suggested that the long-wave effect was smaller by half than the solar effect of cloudiness on net radiation. *Cess et al.* [1982] suggested that the causes for the discrepancy were rooted primarily in the differences in the frequencies of radiation to which the instruments were sensitive. In particular, they noted that cirrus clouds are relatively transparent to radiation in the 10.5- to 12.5-μm region in comparison to longer wavelengths. Thus the NOAA data might be expected to underestimate the outgoing long-wave reduction associated with the presence of cirrus cloud. The 0.5- to 0.7-μm region was chosen for the NOAA satellites specifically for the ability of measurements in this region to discriminate cloud. The contrast between the albedo of cloudy and clear skies maximizes in this region. At wavelengths greater than 0.7 μm, cloud albedos decrease, and the albedo of vegetated land areas increases. One would thus expect the NOAA SR data to overestimate the albedo contrast between cloudy and clear skies. This potential overestimate has been investigated quantitatively by S. G. Warren (private communication, 1981) and *Shine et al.* [1984]. They both find that albedo estimates based on narrow-band measurements from the NOAA SR and very high resolution radiometer (VHRR) instruments would overestimate the cloudy-clear albedo contrast by about 40%. This is not enough to completely explain

the difference between the estimates of cloud forcing of net radiation obtained by *Cess* [1976] and *Cess et al.* [1982] and those obtained by *Ohring and Clapp* [1980] and *Hartmann and Short* [1980]. Further work in this area is clearly needed.

4. THEORETICAL AND MODEL STUDIES

Introduction

Earth radiation budget (ERB) data have two important applications for climate model studies. The first application concerns the development of radiative parameterizations for simple climate models. For example, *Cess* [1976] and *Lian and Cess* [1977] used *Ellis and Vonder Haar*'s [1976] compilation of ERB data and developed parametric equations for the dependence of outgoing long-wave flux on surface temperature and the effect of clouds on planetary albedo, long-wave fluxes, and the ice-albedo feedback effect. These equations have subsequently been reevaluated by other investigators [e.g., *Oerlemans and Van den Dool*, 1978; *Warren and Schneider*, 1979; *Short et al.*, 1984] and used in numerous energy balance model studies (see the review by *North et al.* [1981]) and have provided valuable insights into the climate feedback processes.

The second application of ERB data for models concerns the validation of general circulation models (GCMs) of the climate, which will be the focus of the discussion in this section. The GCMs with coupled ocean-atmosphere and with interactive dynamical-diabatic processes are the most sophisticated tools available for studying the global climate. GCMs are currently being used to study the effect of cloudiness on the sensitivity of climate [e.g., *Hunt*, 1978; *Schneider et al.*, 1978; *Wetherald and Manabe*, 1980; *Shukla and Sud*, 1981; *Liou and Zheng*, 1984; *Hansen et al.*, 1984]. An ERB data set, provided it has sufficient accuracy, can make significant contributions to the validation and the subsequent improvement of the GCMs. The primary model validation objectives (with regard to the ERB data) are to examine the fidelity of the models in simulating the following features: (1) the global, zonal, and regional radiative forcing, i.e., absorbed solar and outgoing long-wave radiation, including the seasonal and interannual variation, of the earth-atmosphere system; (2) the role of interactive processes in modulating the radiative forcing; foremost in importance is the role of clouds in determining the observed radiative forcing, which should not be confused with the cloud radiative feedback; and (3) the internal climate variables that determine the radiative effects of the interactive processes (for example, in the case of the cloud radiative forcing, the relevant variables are cloud fraction, cloud radiative properties, cloud microphysics, and cloud vertical location).

The ERB data, by itself, would be sufficient to accomplish objectives 1 and 2. In what follows, the scientific merits and the strategy for accomplishing objectives 1 and 2 with the ERB data will be described. The last objective (i.e., objective 3 above) requires, in addition to ERB data, a long list of auxiliary data (of sufficient accuracy) such as cloud cover, cloud optical properties, cloud heights and thickness, moisture distribution, and several others. It is desirable to accomplish this objective in the not-too-distant future. However, the order of the three validation objectives is not very crucial. As will be illustrated here, meeting objectives 1 and 2 with ERB data would constitute a big step toward development of comprehensive global climate models.

The validation process should consist of three steps: (1) validation of the radiative transfer scheme used in the climate model; (2) validation of the parameterization of interactive processes, e.g., cloud-radiation interaction; and (3) validation of the model simulation of the global, zonal, and regional energy budget. There are many difficult issues that need to be resolved before attempting the validation process. However, a few major and important issues can be addressed successfully with the aid of a limited period of radiation budget data (such as ERBE), and attention will be focused mainly on these issues. A few concepts that govern the strategy proposed here for validating GCMs with the aid of ERBE data will be introduced. These concepts, described in the next section, are derived from considerations of the top-of-atmosphere radiative energy budget equation.

Clear Versus Cloudy Energy Budget

Consider the top-of-atmosphere radiation budget for a region partially covered by clouds. The region consists of a clear-sky region with a fractional areal extent of $1 - C$ and an overcast fraction C. The entire region consisting of the clear-sky and overcast portions will be denoted as the cloudy region. The spatial resolution of the region, with respect to the ERBE data, varies from about 10^4 (km^2) for the scanner instrument to about 5×10^5 (km^2) for the nonscanner instruments. For such large regions the outgoing long-wave flux F can be written as

$$F^a = (1 - C)F^{cl} + CF^{ov} \tag{20}$$

where the superscripts for the flux F are as follows: *ov* for overcast, *cl* for clear sky, and *a* for average cloudy conditions. It should be noted that F^a is the value typically observed by nonscanning radiation budget instruments, since their spatial resolution is too coarse to detect (with minor exceptions) regions with either complete clear-sky or overcast conditions. After trivial manipulation, (20) can also be written as

$$F^a = F^{cl} - C^f \tag{21}$$

where

$$C^f = C(F^{cl} - F^{ov}) \tag{22}$$

Similarly, the solar radiation S absorbed by the earth-atmosphere can be written as

$$S^a = S^{cl} - C^s \tag{23}$$

where

$$C^s = C[S^{cl} - S^{ov}] \tag{24}$$

The parameters C^f and C^s represent the net effect of clouds on the surface-atmosphere radiative heating and hence will be referred to as the cloud radiative forcing terms. Equations (22) and (24) are written symbolically for a single-level cloud cover and can be generalized to multilevel cloud decks by estimating the terms on the right-hand side of (22) and (24) for the various cloud types and adding the contribution from the individual clouds. The above equations set the stage for formulating a model validation strategy in terms of clear-sky fluxes and the cloud forcing terms.

For a complete verification of the treatment of cloud-radiative interactions a comprehensive data set that includes independent (independent of radiation budget data) estimates of the cloud fraction C, the cloud optical properties, and the atmospheric and surface variables that influence the radiative transfer is needed. This sort of comprehensive model validation is extremely difficult to undertake, and the validation problem is further complicated by the strong dependence of

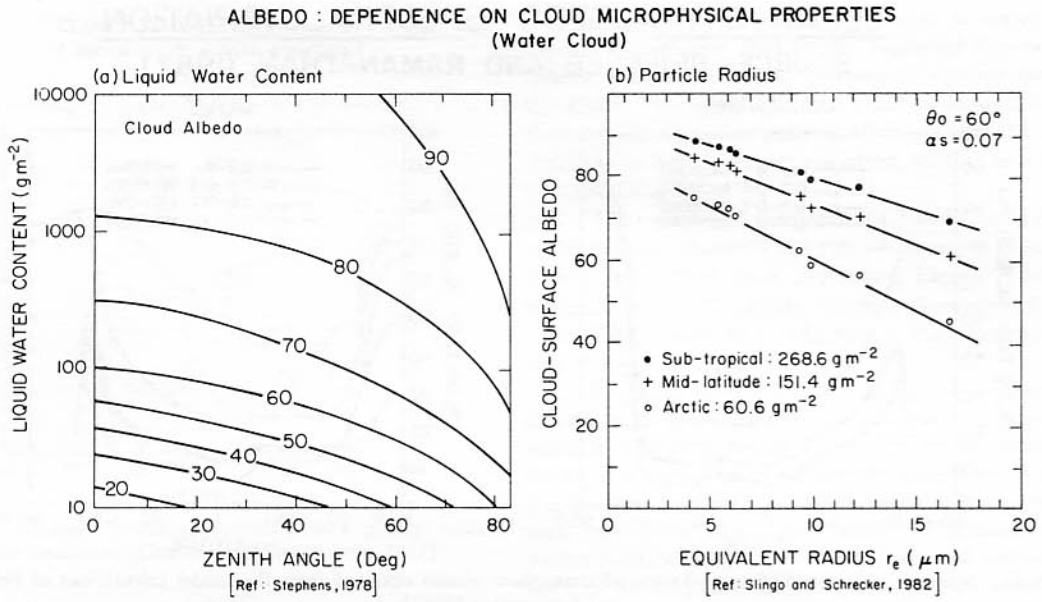

Fig. 9. Dependence of cloud albedo on cloud microphysical properties: (*a*) albedo as a function of zenith angle and liquid water content and (*b*) albedo as a function of equivalent radius. (Redrawn from the references indicated.)

cloud radiative properties on the cloud microphysical parameters. For example, Figure 9 shows the dependence of cloud albedo on cloud liquid water content and zenith angle (Figure 9*a*) and on cloud particle size distribution (Figure 9*b*). In Figure 9*b*, cloud particle size is expressed in terms of the equivalent radius of the size spectrum. The long-wave emissivity of clouds also depends strongly on the cloud microphysical properties as shown in Figures 10*a* and 10*b*. Nevertheless, with the aid of such a comprehensive data set we could compare the various terms in (22) and (24) between models and observations. It is not clear whether such a comprehensive data set with adequate accuracy will be made available during the ERBE period. Even if such a data set were to be made available, it might include only limited regions of the globe. There is a more direct way of obtaining the cloud radiative forcing, however, which from (21) and (23) can be written

$$C^f = F^{cl} - F^a \tag{25}$$

$$C^s = S^{cl} - S^a \tag{26}$$

Hence the radiative forcing of clouds can simply be obtained as a difference between the measured values for clear-sky and for average cloud conditions without undertaking the arduous task of measuring cloud cover and other auxiliary data. This, by itself, would be a significant step, since it is the radiative forcing that influences the climate and the general circulation. Furthermore, the cloud radiative forcing terms as expressed in (25) and (26) involve differences between two sets of measurements taken over the same region at nearly the same time interval. Consequently, any instrumental errors that degrade the absolute accuracy will not impact the estimates of C^f and C^s, provided the instrument has acceptable precision (i.e., relative accuracy). However, (25) and (26) do require an accurate determination of clear-sky values, but these are easier (at least conceptually) to obtain from both measurements and models. In what follows, the nature of the clear-sky fluxes and the cloud forcing terms as inferred from climate models will be considered, and the key issues that can be addressed with the aid of ERBE data illustrated.

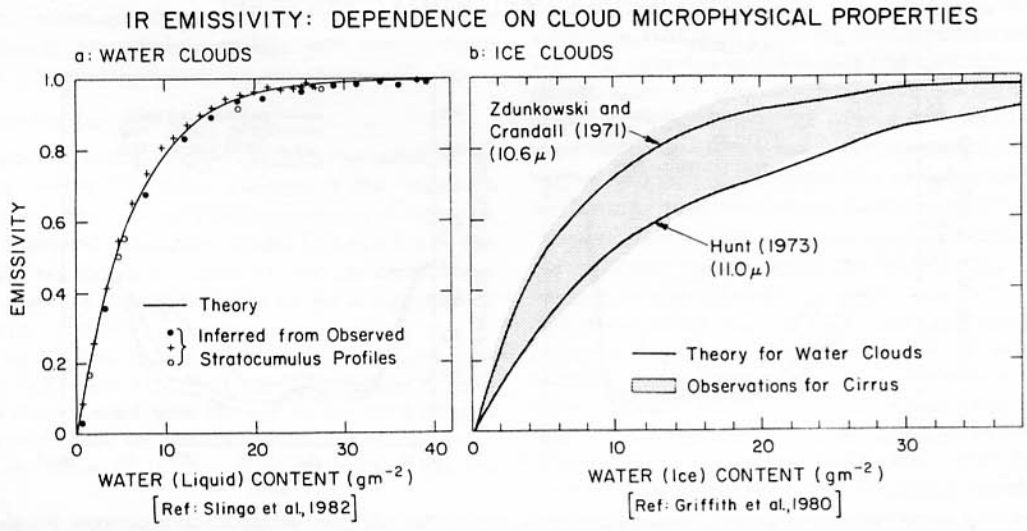

Fig. 10. Dependence of cloud emissivity on cloud water content: (*a*) water clouds and (*b*) ice clouds.

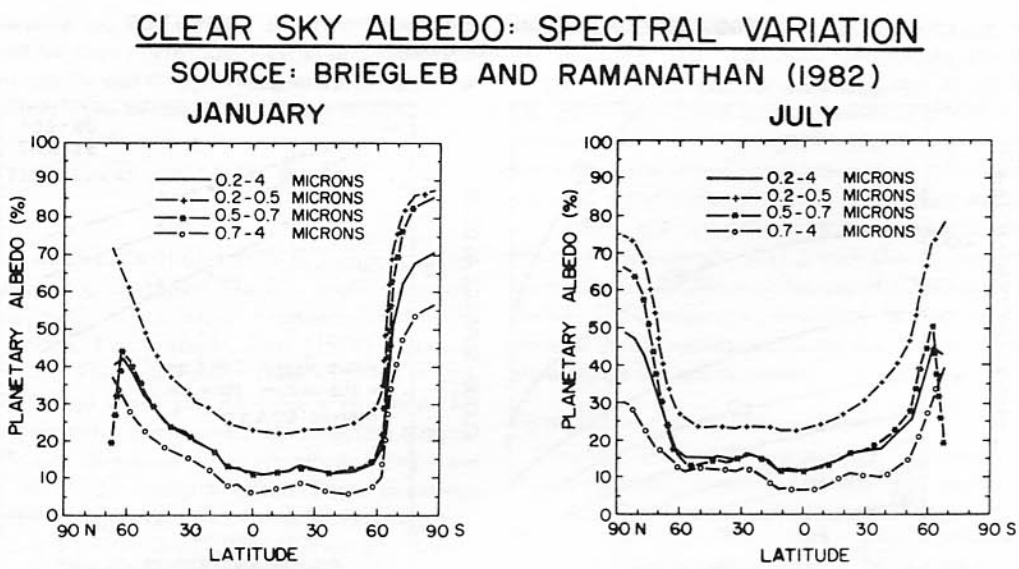

Fig. 11. Spectral dependence of clear-sky top-of-atmosphere albedo obtained from the model calculations of *Briegleb and Ramanathan* [1982].

Clear-Sky Fluxes

Ideally, the first step toward validating clear-sky climatology should be to verify the radiative transfer schemes used in climate models. In order to verify the radiation model one must specify the optically active atmospheric constituents, temperatures, and the surface optical properties, i.e., albedo and emissivity. This step can be done for selected soundings, provided the necessary auxiliary data set (e.g., H_2O distribution) is available. Model verification of this sort has been attempted [e.g., *Ellingson and Gille*, 1978]. In addition, currently there is an international effort cosponsored by the International Radiation Commission and the World Meteorological Organization (WMO) to intercompare parameterized radiation codes (used in climate models) with detailed line-by-line calculations. More than 20 major research groups have been involved in this intercomparison study, which culminated in a workshop in August 1984. This procedure, while it does not verify models with observation, will test the validity of several approximations (e.g., Curtis-Godson scaling) employed in radiation codes used in climate models. This intercomparison study will enable us to calibrate the radiation treatment in climate models against line calculations which in turn have been calibrated with the laboratory and atmospheric transmittance data. In any case, the validation of the radiative transfer model should be undertaken independently of the ERB data.

The clear-sky albedo at the top of the atmosphere will be used to illustrate the issues that can be addressed with the aid of broadband ERB data. As shown in Figure 11, the clear-sky albedo has a strong spectral variation because of the spectral variations in atmospheric absorption, in scattering, and in the surface reflectivities. The zonal average results shown in Figure 11 are obtained from model calculations on a two-dimensional latitude-longitude grid of 500 × 500 km. The calculations account for the regional variations in vegetation, soil, snow, sea ice, and ocean reflectivities but ignore the subgrid scale variations in surface reflectivities. Such subgrid scale variations in surface reflectivities arise because of the strong dependence of surface reflectivities on vegetation types, soil moisture, and the surface roughness. The situation is further

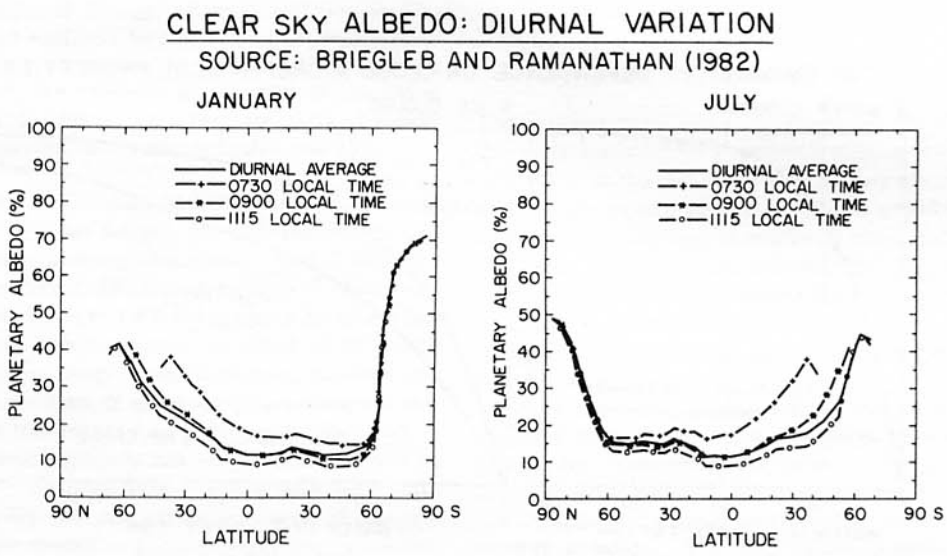

Fig. 12. Diurnal variation of clear-sky top-of-atmosphere albedo obtained from the model calculations of *Briegleb and Ramanathan* [1982].

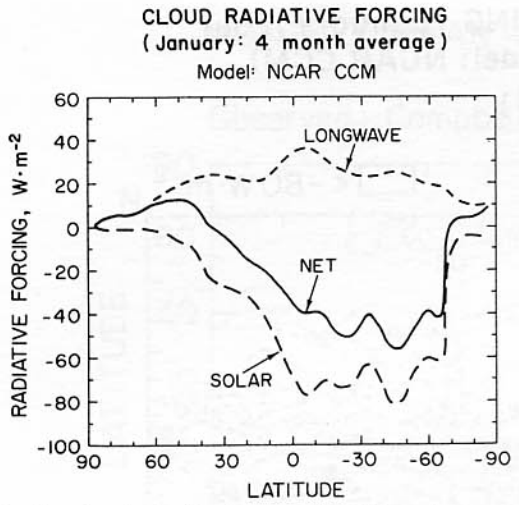

Fig. 13. Cloud radiative forcing as derived from a general circulation model simulation [*Charlock and Ramanathan*, 1985].

complicated by the strong spectral dependence of the reflectivities. It is very difficult, if not impossible, to specify a broadband surface reflectivity for a model grid box with dimensions of about 500 × 500 km based on a precise spatial and spectral averaging process. Hence the comparison of the clear-sky broadband albedos with observations would be valuable for validating the climate model practice of specifying a bulk albedo over a large region. Also to be noted from Figure 11 are the strong seasonal variations in the albedos. In view of the spectral dependence of the albedos shown in Figure 10 it is clear that albedos derived from narrow-band instruments are not sufficient to validate models.

The second key issue concerns the diurnal variation of the clear-sky albedos. Model results for the diurnal variation are shown in Figure 12. The computed diurnal variations shown in Figure 12 arise from the zenith angle dependence of atmospheric scattering, atmospheric absorption (since the optical path length is inversely proportional to the cosine of the zenith angle), and surface reflectivity. Although only zonal mean results are shown, the model calculations are performed on a longitude by latitude grid. A comparison of the computed and observed diurnal variation in the albedo would enable one to assess the model treatment of the zenith angle dependence of surface reflectivities over the whole globe. As mentioned earlier, in view of the strong spectral dependence of the surface reflectivities and the atmospheric optical properties it is not sufficient to compare models with narrow-band measurements.

Cloud Radiative Forcing

Model calculations can be used to examine the nature of the cloud radiative forcing. The zonal averages of the long-wave (C^f), solar (C^s), and net ($C^s - C^f$) radiative effects of clouds as simulated by a general circulation model [*Charlock and Ramanathan*, 1985] are shown in Figure 13, and the corresponding regional values are shown in Figure 14. As is expected, C^f is highly positive.

The results in Figures 13 and 14 reveal several important and interesting features of the cloud radiative forcing. If these features could be validated with the aid of the ERB data, it would considerably improve our understanding of the cloud-climate problem. Some of the more interesting features are listed here.

1. The relative magnitudes of C^f and C^s and the net effect of clouds on a hemispherical-seasonal mean scale indicate whether clouds on a global scale cool or warm the planet. Figure 13 indicates that in the National Center for Atmospheric Research (NCAR) community climate model (CCM) the global long-wave trapping effect of cloudiness is smaller than the shortwave reflectivity effect, so that the net effect of clouds is to reduce the net radiation, leading to a cooler equilibrium climate.

2. The meridional gradients in C^f and C^s and their seasonal dependence illustrate the role of clouds in determining the tropospheric zonal mean circulation. Figure 12 indicates that the net effect of cloudiness, which is dominated by the shortwave effect, results in a reduction in the required equator-to-pole energy transport.

3. Regional variations in cloud forcing indicate the role of cloudiness in establishing regional climate and controlling the required east-west energy transports in the atmosphere and ocean. It is seen (Figure 13) that the long-wave effect of clouds is maximum in the ITCZ zonal belt, and from Figure 14 it is seen that C^f is larger over preferred locations such as the winter monsoon region over Indonesia and the southern portions of the mid-latitude jet streams (see the large values over the southeastern coast of the United States and over the southern coasts of China). Similarly, the solar effects have preferred latitudinal and regional locations. It is clear that the cloud forcing term, as simulated in the model, has signatures in the form of zonal and regional asymmetries which are so strong that it should be relatively easy to identify them from the satellite data set and validate the model simulations.

Regional Energy Budget

There have been numerous attempts (*Geleyn et al.* [1982] and *Slingo* [1982], to name a few) to compare the radiation budgets computed by GCMs with observations. Two examples are shown in Figures 15 and 16. It is clear that there are major regions of agreement and regions of disagreement between the two. The main questions are how the model performance should be assessed, and more importantly, what procedures should be adopted to make improvements in the model simulation. For example, the differences may arise from a number of deficiencies: errors in prescription of surface properties, errors in the GCM simulation of H_2O and temperature, errors in the cloud treatment, and several others. In order to sort out these questions a necessary first step is to compare the clear-sky fluxes and the fluxes with clouds. Figure 17 shows model simulations of these two quantities for the outgoing long-wave flux. It is interesting, and perhaps not surprising, that most of the regional asymmetries in the outgoing long-wave flux in the tropics and subtropics are caused by clouds, since the clear-sky flux variations with longitude are considerably smaller in the tropics and subtropics. With respect to the long-wave flux, clear-sky comparison with observations will isolate the errors due to deficiencies in H_2O and temperature simulations from those due to clouds.

Another important issue that should be dealt with concerns the statistical significance of the results. This question arises because of the inherent variability ("noise") in the internal climate variables (e.g., H_2O, clouds, and temperature). For example, Figure 18 shows the standard deviation of the monthly mean outgoing long-wave flux estimated from observation (the NOAA 10- to 12-μm narrow-band data) and from model calculations. Because of the large variability revealed both in the observations and in the model simulation, the statistical significance of the differences should be assessed before objectively interpreting differences between models and observations.

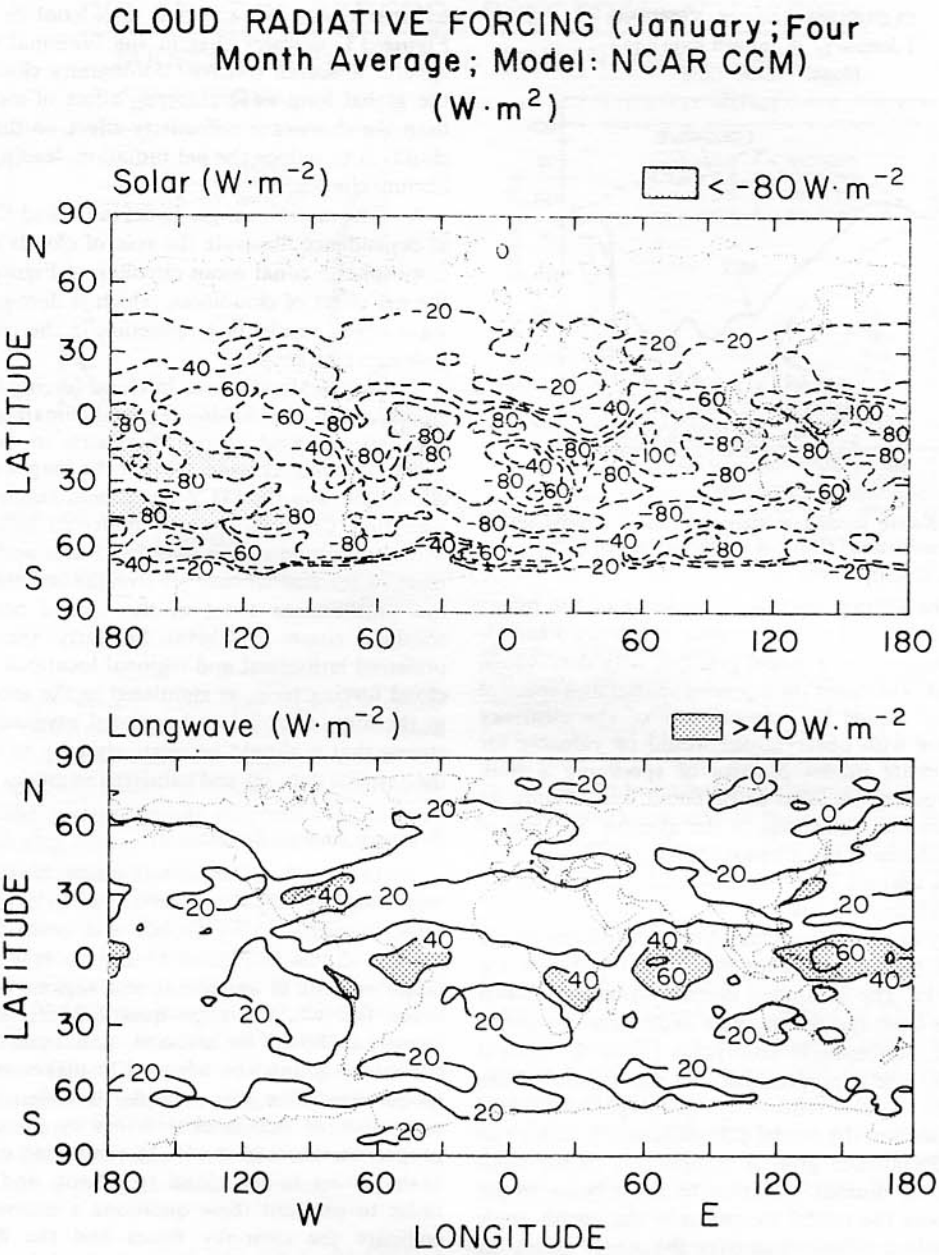

Fig. 14. Regional cloud radiative forcing as derived from a general circulation model simulation [*Charlock and Ramanathan*, 1985].

Validation of General Circulation Models

A strategy has been described which involves validation of the clear-sky fluxes, followed by validation of the cloud radiative forcing, and culminating in scrutinizing the regional radiation budget for average cloudy conditions. It is appropriate at this stage to consider an example of how this strategy will enable a better understanding of the behavior of the model and, if the model is realistic enough, ultimately lead to a better understanding of the actual climate system.

In Figure 19 the zonally averaged outgoing long-wave flux obtained with several versions of a GCM are compared [see *Ramanathan et al.*, 1983]. The GCMs used for the three curves shown in Figure 19 are identical but for the treatment of cirrus clouds. The control experiment has no clouds above 250 mbar. In a second experiment the cirrus emissivity is treated as black, while in the third a variable cirrus emissivity that depends on the cloud liquid water content is incorporated. Restricting attention to the region between 30°N and 30°S, it is seen that the high-level clouds have a significant impact on the outgoing long-wave flux. Furthermore, the model simulation of upper tropospheric temperatures and zonal jet strength (not shown here) depend very strongly on the treatment of cirrus clouds. Although the model version with variable cirrus emissivity shows the best agreement with observations, it would be premature to choose this version of the model over the others solely on the basis of the results shown in Figure 19. There are several reasons for this difficulty. A few important ones are that (1) it is possible that the model biases in clear-sky fluxes are comparable to the cirrus effects shown in Figure 19; (2) the natural variability in outgoing long-wave flux due to cloud variability may be as large as the differences shown in the figure; and (3) there are possible errors in the cloud radiative forcing due to low- and midlevel clouds. Several difficulties mentioned above can be ruled out by comparing the clear-sky and cloud radiative forcing individually. One can compare the effects of cirrus cloud on the radiation

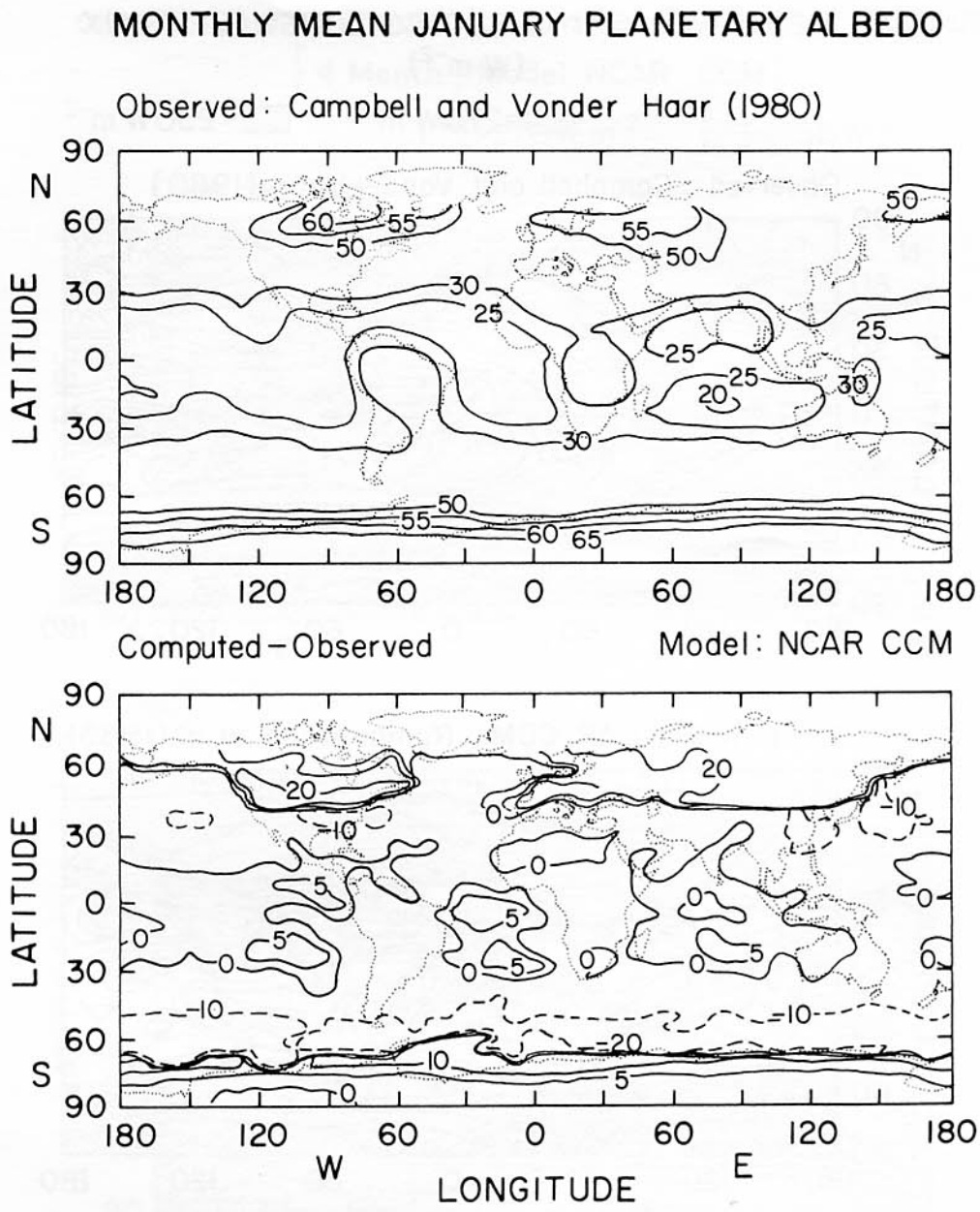

Fig. 15. Monthly mean January planetary albedo: (top) observed, and (bottom) difference between computed and observed. The computed values are from the GCM results of *Ramanathan et al.* [1983].

budget of regions where the cirrus effects are manifest (e.g., tropical convective region and winter monsoon region). After such validations are completed, comparison of zonally averaged fluxes (for averaged cloudy conditions) will constitute a rigorous test of the hypotheses that are being tested through a model-observation intercomparison study. In the example shown in Figure 19 there are two important hypotheses that can be tested. The first concerns the importance of cirrus to the radiative heating of the tropical region, and the second concerns the emissivity of cirrus clouds for climate studies. These are important issues for both the general circulation and the climate sensitivity problems. The example given above is only one of many that can be cited to illustrate the contributions that a carefully planned model validation study (with ERB data) can make to the climate field.

Diagnosis of Numerical Weather Prediction Models

Modern numerical weather prediction models, particularly those intended for forecasts beyond a few days, include diabatic processes such as latent heat release and radiation. The methods used to incorporate diabatic processes in weather prediction models vary in complexity. It is important to evaluate accurately the relative effectiveness of each method. The accurate modeling of radiation and cloud-radiation interaction is recognized to be of paramount importance for climate simulation [*Oxford GARP Study Conference*, 1979]. The question arises whether proper simulation of clouds and radiation is important for short- and medium-range weather forecasting.

The usual way to investigate the importance of the parameterization of one particular physical process is to make parallel integrations with numerical models, differing only by the scheme which represents that effect. However, the diagnostic tools used to compare model simulations do not always allow unambiguous conclusions to be drawn. *Cubasch* [1981] compared 10-day forecasts with the operational model of the European Center for Medium Range Weather Forecasting (ECMWF) using three different radiative schemes. He found

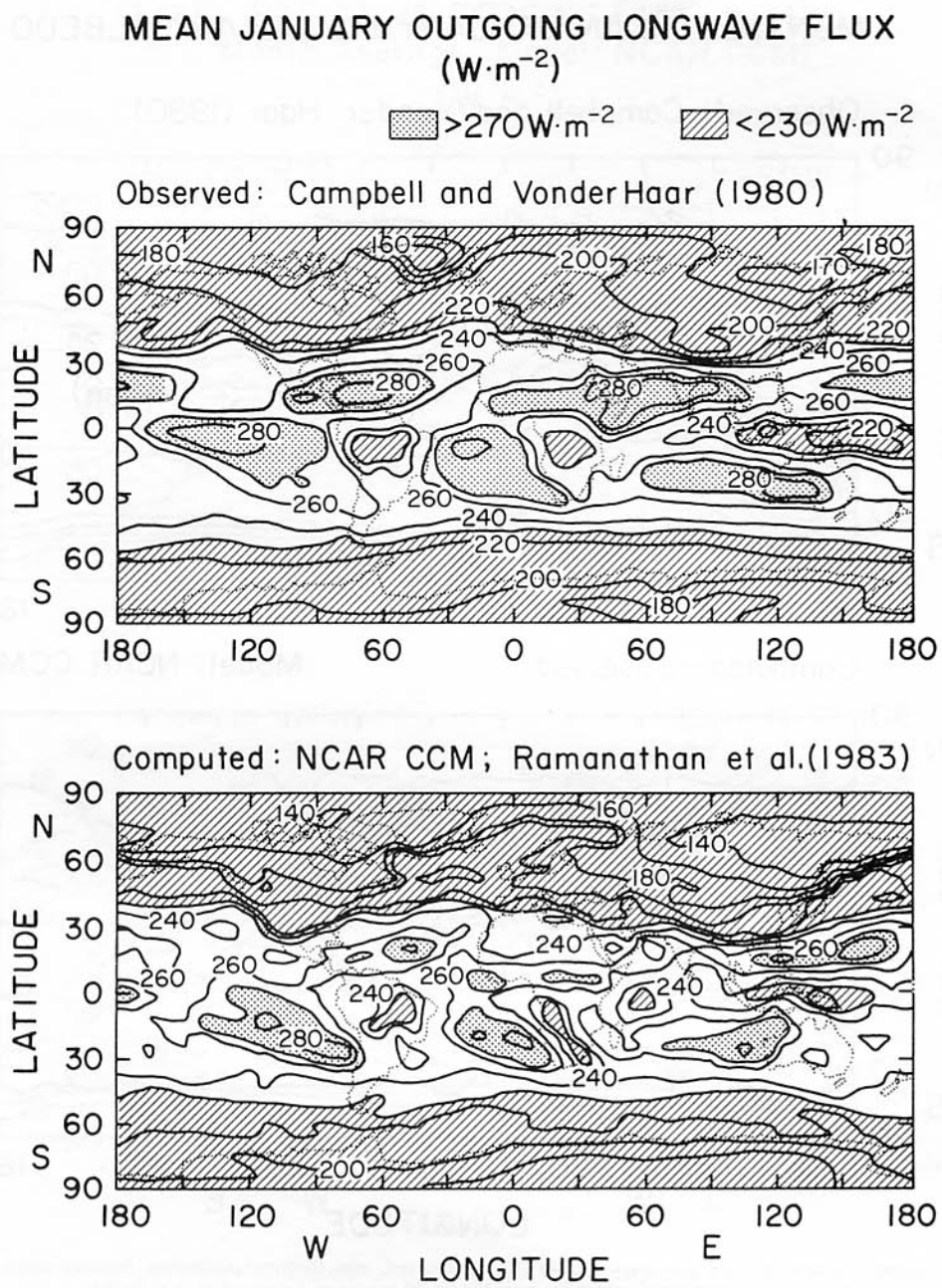

Fig. 16. Comparison of (top) observed values and computed values of outgoing long-wave flux.

only minor and nonsystematic differences on the height field (as long as they compare reasonably well with the analyzed fields), and therefore the forecast skills were not different, although some differences in the model's energetics were apparent.

The direct comparison of radiation fields at the top of the atmosphere computed by the model with those deduced from measurements appears to be a better tool for revealing the differences between radiative schemes and for analyzing their qualities and defects. However, the complex nature of the radiation-dynamics interaction and the possibility of intricate self-regulating mechanisms during the integration may make it difficult to isolate the effects of radiative schemes from all the other possible influences.

Geleyn et al. [1982] and *Morcrette and Geleyn* [1985] used the operational model of ECMWF in several versions differing only in the radiative schemes. They compared the radiation fields at the top of the atmosphere to the same fields derived from measurements by NOAA 4 for February 1976 and by TIROS-N for January 1979 [*Winston et al.*, 1979]. The data set provided by NOAA is based on the scanning radiometer (SR) measurements for NOAA 4 and on the advanced very high resolution radiometer (AVHRR) for TIROS-N. The total outgoing long-wave flux is estimated from the infrared radiances measured in the IR channel of SR (10.5–12.5 μm) or in channel 4 of AVHRR (10.5–11.5 μm) by a nonlinear regression method based on radiation calculations for a set of different atmospheres [*Gruber and Winston*, 1978; *Gruber et al.*, 1983]. The shortwave reflected flux is determined directly from the radiances measured in the visible channel of SR (0.5–0.7 μm) or in channel 1 of AVHRR (0.58–0.68 μm) without any correction for anisotropy or diurnal variations.

Quantitative comparisons were made either on zonally averaged 10-day mean values or on globally averaged, time

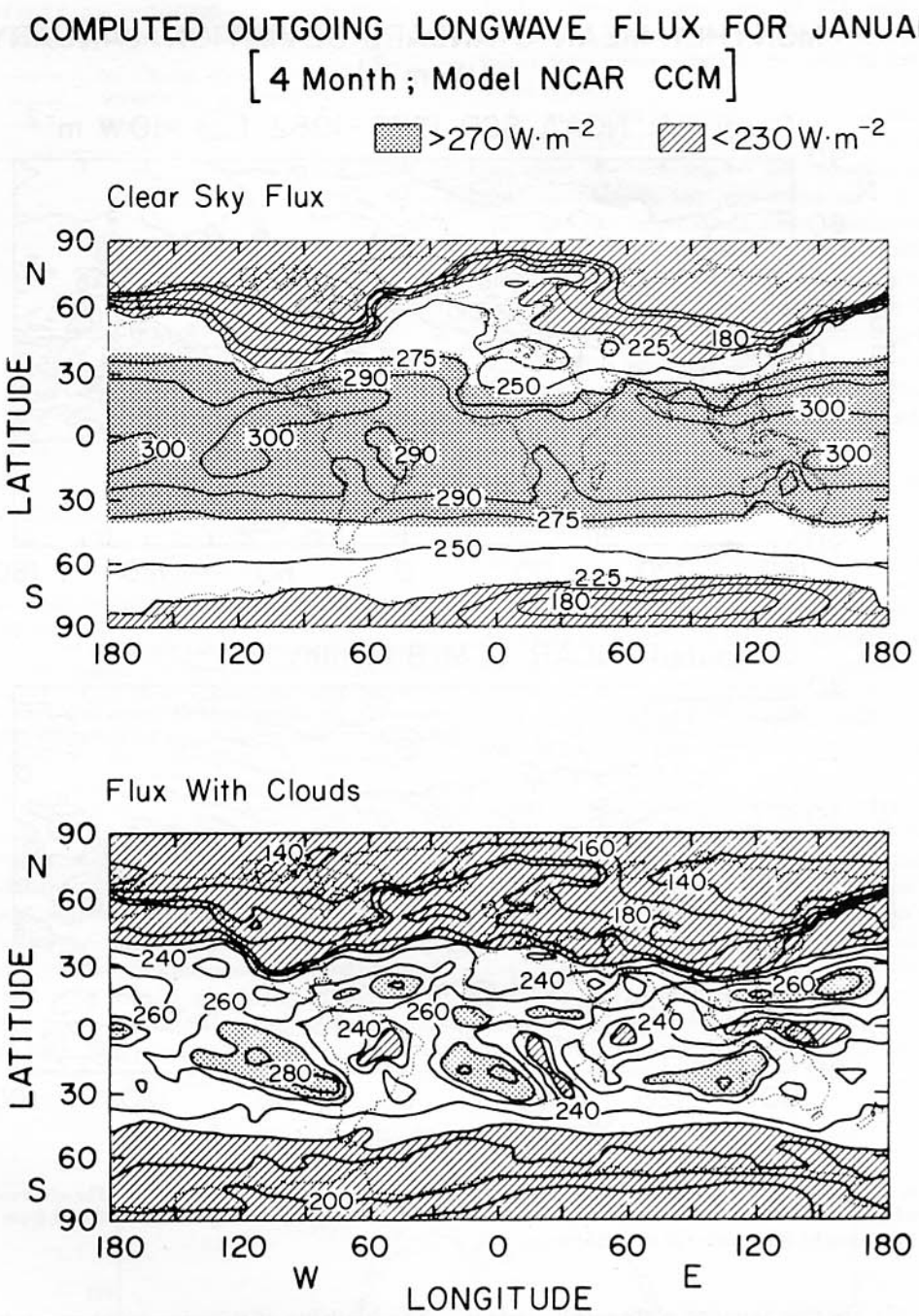

Fig. 17. Comparison of clear-sky and cloudy-sky outgoing long-wave fluxes. These results are taken from the GCM results shown in the work by *Ramanathan et al.* [1983].

dependent values. The zonally averaged 10-day mean values of long-wave emission show overall good agreement between models and satellite data (Figure 20) with the exception of the tropical belt where the ECMWF model, whatever radiation scheme is used, is deficient. *Geleyn et al.* [1982] relate this deficiency partly to the cloud-radiation interaction in the model and partly to an underestimate of cumulus cloud by the cumulus parameterization in the model. The zonally averaged 10-day mean values of albedo are also in satisfactory agreement (Figure 21) if one takes into account the fact that the satellite data may be biased toward high values over snow and clouds because of the representation of the whole shortwave spectrum by a narrower channel [*Slingo*, 1982]. For net radiation the discrepancies are larger, reaching ± 40 W m^{-2} in some regions for one radiation scheme and more than 60 W m^{-2} for another. It is not considered productive to attempt to allocate these discrepancies to particular causes, since the overall quality of these satellite data remains in doubt. The much higher quality expected for the ERBE data set should open many possibilities for deeper analysis of such comparisons.

The comparison of the computed and observed global radiation balance components as functions of time can provide insight into the details of parameterization schemes. For example, the two versions of the ECMWF forecast model, studied by *Geleyn et al.* [1982], exhibit very different drift patterns for infrared radiation and planetary albedo. In contrast, the drift of net radiation is the same, within ± 1 W m^{-2}, in the

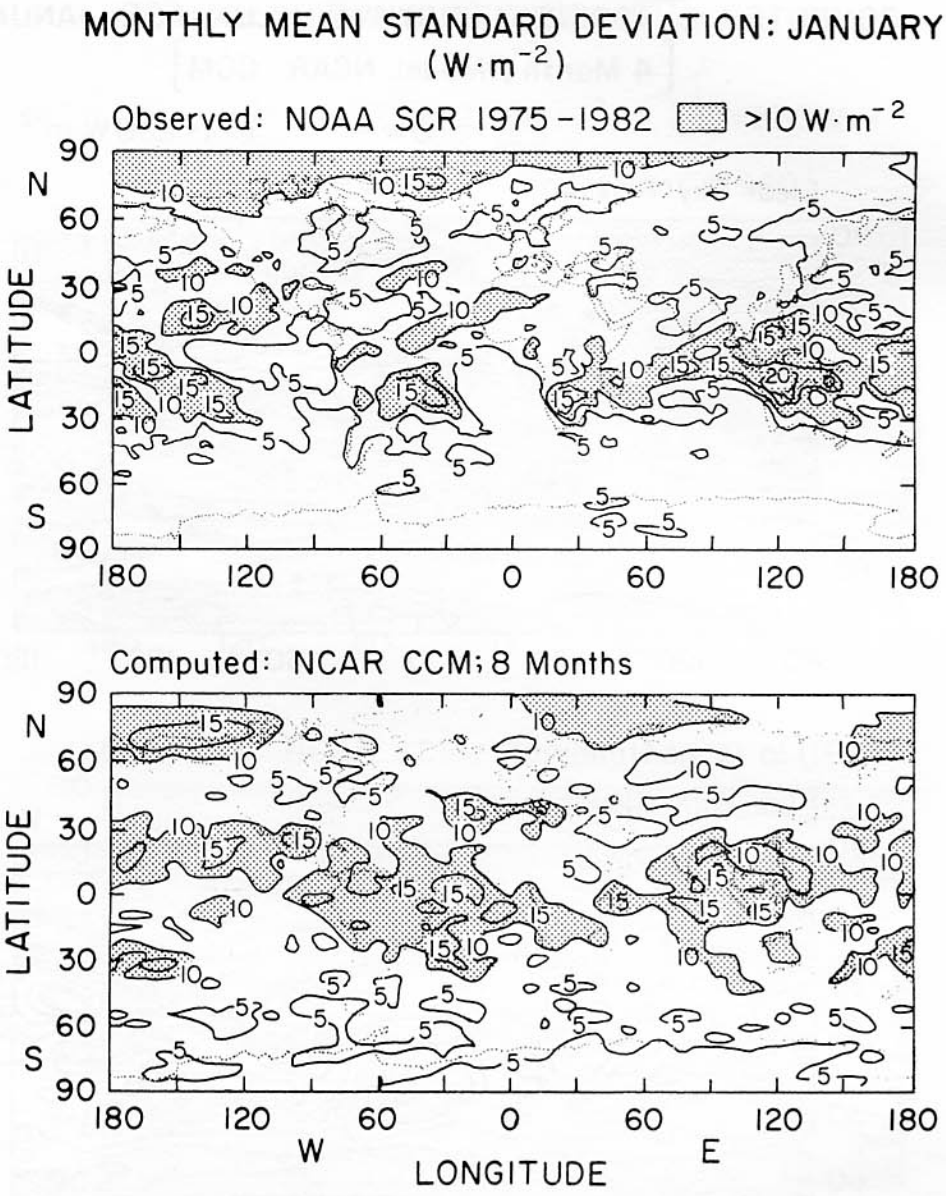

Fig. 18. Comparison of the monthly mean standard deviation in the outgoing long-wave flux. The observed deviation is inferred from the data described in the work by *Gruber* [1978]. The computed values are obtained from the results shown in the work by *Ramanathan et al.* [1983].

two cases (Figure 22). The time variation of the satellite data is different from that of both of the model data sets, however. If higher confidence could be put on the value of the satellite data, this type of comparison could provide a judgment as to which scheme is better.

Daily ERBE data will be useful for scientists wishing to conduct research on the representation of planetary waves by numerical weather prediction and general circulation models. It is well known that the planetary waves are rather poorly simulated in general circulation models, although the reasons for this failure remain unclear.

Among various experiments which can be considered, those dealing with the sensitivity of planetary waves to misrepresentations of the forcing seem most promising. Radiation budget data, properly forced into a numerical model, could result in an improvement of the planetary scale forcing, the impact of which could be felt at the level of planetary wave simulation. The feasibility of this experiment proceeds from the two following considerations: (1) planetary scale radiative forcing at the top of the atmosphere can be inferred from ERBE data with high enough resolution in time; and (2) the vertical structure of the radiative forcing may be of secondary importance, since the dominant planetary waves tend to have simple vertical structures. An accurate assessment of the effect of diabatic heating on the low-frequency variability of planetary waves would constitute an important contribution to the extended range forecasting problem.

5. Relation of ERBE to ISCCP

The International Satellite Cloud Climatology Project (ISCCP) has been organized within the framework of the World Climate Research Program (WCRP) to collect and

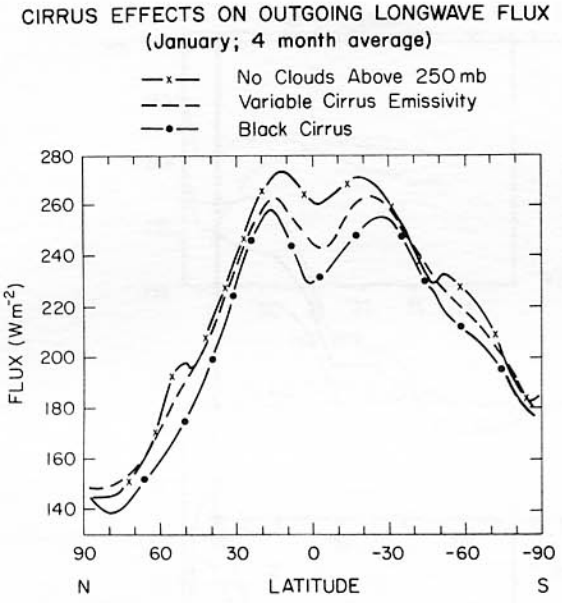

Fig. 19. Effect of cirrus clouds on computed outgoing long-wave flux. Observed values are from the work by *Campbell and Vonder Haar* [1980]. The computed values are taken from the GCM results of *Ramanathan et al.* [1983, Figure 21]. The Control curve (curve with crosses) has no clouds above 250 mbar. The dashed curve has clouds up to 100 mbar, but the cloud emissivity is dependent on the model-generated cloud water (ice) content; the dash-dot-dash curve is the same as the dashed curve, but the cirrus emissivity is assumed to be black.

analyze satellite radiance data to infer the global radiative properties of clouds and improve the modeling of cloud effects on climate [*World Climate Program*, 1982; *Schiffer and Rossow*, 1983]. The operational component of ISCCP aims at producing a 5-year global satellite radiance and cloud data set for the period 1983–1988, taking advantage of the global coverage provided by polar-orbiting and geostationary meteorological satellites. The primary data will be the standard visible (6.6 μm) and IR (11 μm) channels roughly common to all the satellites. Secondary data will also be collected from other spectral channels to aid in distinguishing cloud types.

As mentioned in section 3, the simultaneous availability of ERBE and ISCCP data will facilitate observational studies of the effect of cloudiness on the radiation budget which were not possible with any preexisting data sets. In particular, if ISCCP is able to provide a useful decomposition of cloudiness into well-defined cloud types, the ambiguities associated with a poorly known scene will be significantly reduced. If, in addition, the cloudiness parameters provided by ISCCP can be related to cloudiness parameters defined in general circulation models, then some of the more detailed model verification studies suggested in section 4 can be attempted by using a combination of ERBE, ISCCP, and conventional data.

6. Solar Constant Monitor

The ERBE packages on the Earth Radiation Budget Satellite and on the NOAA-F and NOAA-G operational spacecraft will each contain a total solar flux detector based on the active cavity radiometer design of *Willson et al.* [1981]. The solar detectors on ERBE will provide an instantaneous digital resolution of 0.02%, and six to seven independent samples of solar irradiance per solar observation will be obtained during the drift of the sun through the solar monitor field of view. The current observing plan is for a solar observation once per month for each satellite.

The solar monitor of ERBE has been designed to provide the $\pm 1\%$ solar irradiance input observations required for earth radiation budget analysis; its accuracy and the number of observations it will give are not sufficient to meet long-term monitoring requirements (0.1%). It is also not capable of detecting the variations of solar irradiance on time scales shorter than 1 month [e.g., *Smith et al.*, 1983]. However, the data of the three instruments may contribute to augment the record of solar irradiance established from the data of the Solar Maximum Mission and provide independent data for comparison.

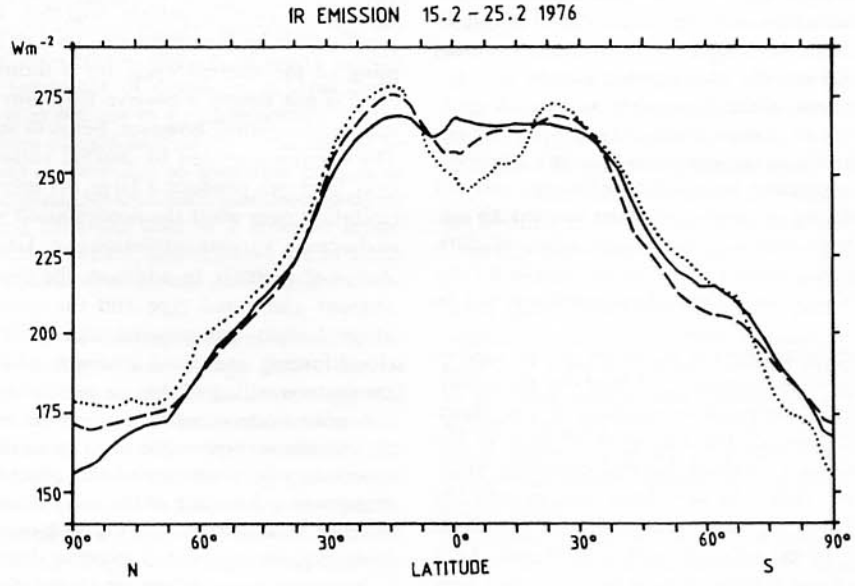

Fig. 20. Zonal and time mean long-wave emission for NOAA 4 measurements for the February 15–25, 1976, period (dotted curve) and long-wave emission averaged over a 10-day ECMWF model forecast starting on February 1979, using two different radiation schemes (solid and dashed curves) [after *Geleyn et al.*, 1982].

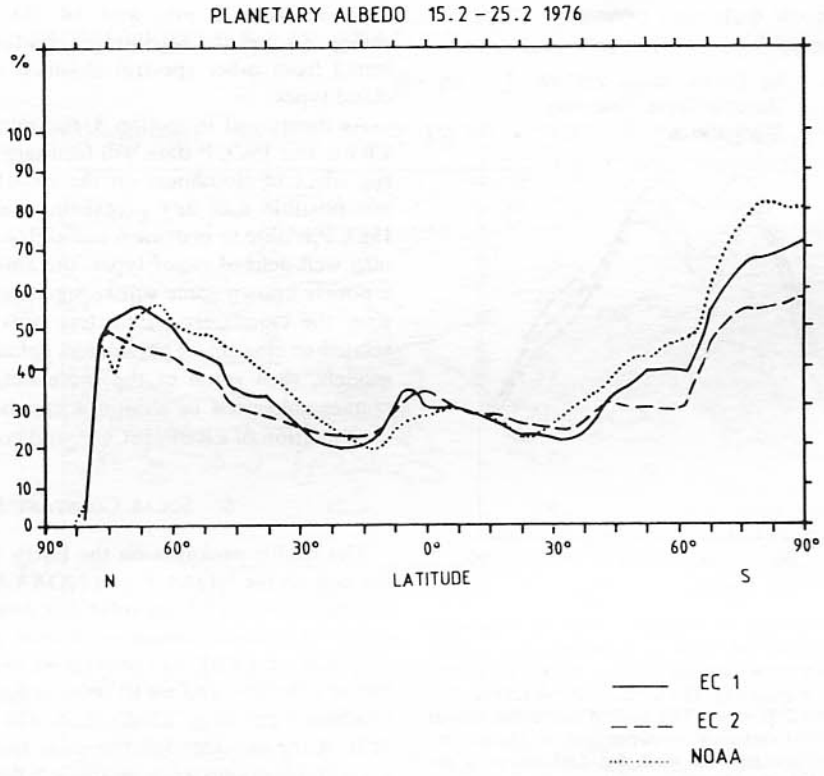

Fig. 21. Same as Figure 20 except for planetary albedo.

7. Summary and Discussion

In this paper the uses of observations of broadband radiative energy fluxes at the top of the atmosphere in scientific studies of weather and climate have been discussed. Observational studies of regional energy balances and of the effects of clouds on the radiation balance and the use of radiation budget data in testing numerical models of the atmosphere have each been highlighted.

Global mean radiation budget components show very interesting annual variations. The net radiation balance of the earth has an annual variation with an amplitude of about 10 W m^{-2}. The global mean net radiation has its largest values near the December solstice. The global mean albedo also has a maximum near the time of the December solstice. A complete understanding of how continentality, cloudiness, and the eccentricity of the earth's orbit contribute to the observed variations in albedo, outgoing long-wave radiation, and net radiation would constitute an important step toward an understanding of the way orbital parameters affect climate. Global measurements with sufficient precision, temporal sampling, and spatial resolution to address these questions will be provided by ERBE.

Annually and zonally averaged net radiation can be used to infer the required poleward transport of heat by the atmosphere and ocean. If an independent estimate of the atmospheric transport is employed, the transport of heat in the oceans can be inferred as a residual. Several currently available estimates of the net radiation have been used to infer the required transport. These do not agree sufficiently well to allow total transport to be inferred with confidence. As a result, inferences of oceanic transport must be assigned a very large uncertainty.

The thermal contrasts between land and sea are important not only in determining the climate over land but also in determining the global climate and its sensitivity. The accurate, high spatial resolution broadband fluxes from the ERBE scanner will allow an adequate discrimination between land and sea areas for climate research.

There are large diurnal variations in the radiation budget components because of zenith angle effects on the reflection of solar radiation and because of systematic diurnal variations in surface temperature, cloud amount, and cloud type. These large diurnal variations represent a sampling problem for polar-orbiting satellites that pass over a given region on the equator only twice a day. ERBE will employ a medium-inclination ($\sim 57°$) orbiter together with one or two sun-synchronous polar orbiters ($\sim 98°$) to obtain a complete sampling of the diurnal cycle on a monthly basis. The diurnal cycle is not simply a passive variation which can be averaged out and forgotten, however, but is of scientific interest in itself. The stirring provided by diurnal variations in surface heating over land can produce a large net increase in continental precipitation over what the precipitation would be in the absence of diurnally varying insolation (e.g., GCM experiments by *Randall et al.* [1985]). In addition, the diurnal variations in cloud amount and cloud type and the associated changes in radiation budget components can provide information about cloud forcing and cloud feedback which may be applicable to the understanding of climate sensitivity.

A poor understanding of the role of clouds in determining the climate is responsible for a large fraction of the remaining uncertainty in estimates of the effect on the climate of such changes as a doubling of the CO_2 concentration. A substantial increase in atmospheric CO_2 and other radiatively active industrial gases is expected to occur during the next century and to have significant effects on global climate and sea level [e.g., *Carbon Dioxide Assessment Committee*, 1983]. Clouds play a central role in determining the relationship between surface climate and top-of-atmosphere energy fluxes. ERBE data can

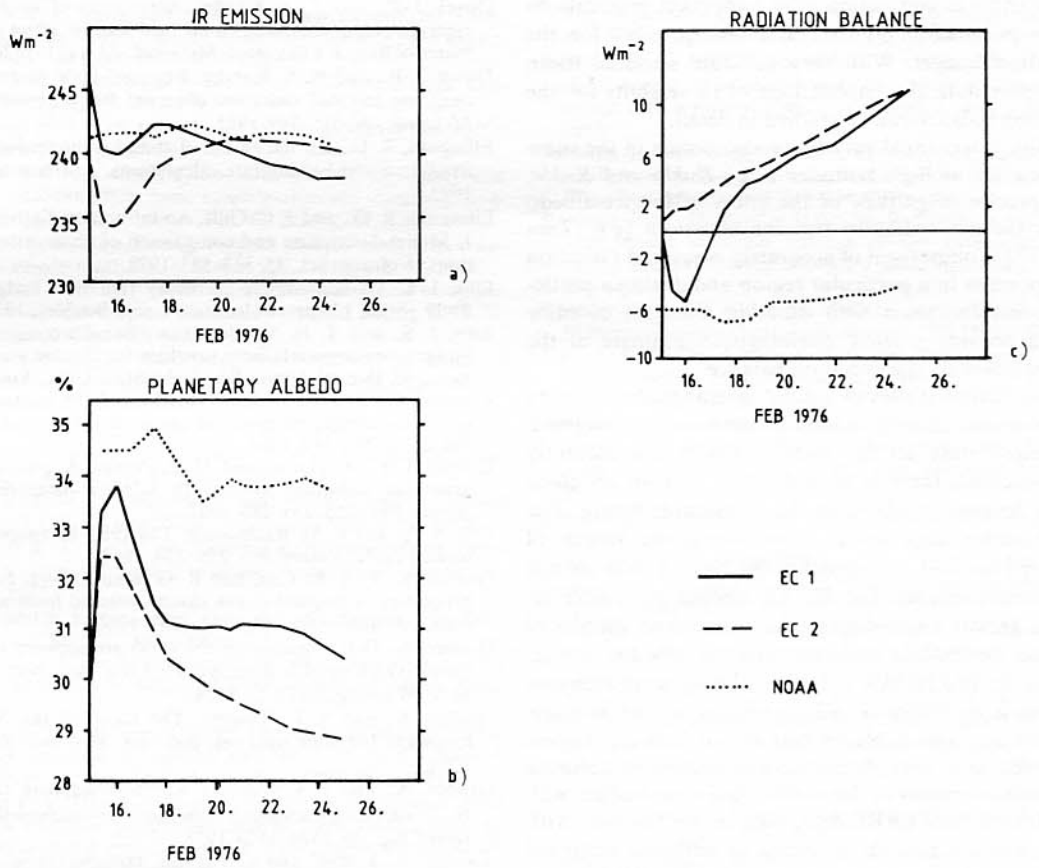

Fig. 22. Time history of the global mean radiation budget components over the 10-day period of February 15–25, 1976; (*a*) long-wave emission, (*b*) planetary albedo, and (*c*) net radiation [after *Geleyn et al.*, 1982]. Line patterns have the same significance as in Figure 19.

be used to investigate this relationship. The availability of cloudiness data from the International Satellite Cloud Climatology Project for the same period during which ERBE measurements will be taken will provide an unprecedented opportunity to study the role of clouds in climate.

The elements of an understanding of climate must be incorporated into the most sophisticated climate models so that the best estimates of the future climatic impacts of man's actions can be obtained. The treatment of clouds in general circulation models (GCMs) is at present in a rather primitive state. The dynamics and physics of each individual cloud cannot be explicitly calculated, and so recourse to ensemble models or parameterization is required. Several such parameterizations are currently in use, and each can lead to a different model climate sensitivity. To test, compare, and improve GCM simulations of the climate requires appropriate observations of the earth's climate.

The simulation by GCMs of the important relationship between climate and top-of-atmosphere energy fluxes can be tested with ERBE data. In this paper it has been suggested that an unambiguous comparison can be made between observed and simulated "average" and "clear-sky" conditions. An accurate estimate of the observed clear-sky radiation budget components can be obtained from the ERBE scanner instrument whose narrow field of view makes the observation of a cloud-free scene a possibility. The comparison of average and clear-sky radiation budget components yields the cloud forcing of the radiation budget for both the model clouds and the observed clouds.

Throughout this paper, attention has been focused almost exclusively upon top-of-atmosphere radiation budget components. For many problems, however, it is equally important to know the radiation budget at the interface between the atmosphere and the surface. Certainly, the combination of an accurate top-of-atmosphere radiation budget with a surface energy budget would open many more opportunities for productive scientific studies. Increasing attention is being focused on ways to infer surface energy budgets from space. Under certain conditions, surface albedo and surface net radiation can be inferred with useful accuracy from top-of-atmosphere measurements [e.g., *Pinker et al.*, 1985]. The estimation of surface radiation budget components from ERBE data, possibly in combination with other satellite-based data, may constitute yet another important scientific application for this data set.

In this paper we have emphasized those important scientific problems which can be addressed with a highly accurate radiation budget data set of 2 or 3 years' duration. There is in addition a set of problems for which an observation period of only 2 or 3 years is of very limited value. These problems have to do with interannual variability, low-frequency variability within a season, and long-term trends of natural or anthropogenic origin. These are problems of great practical as well as theoretical interest which have received increased attention in recent years.

Interannual variability can be used as an important tool for understanding the mechanisms of climate change. As mentioned in section 3, major shifts in the position and intensity of tropical cloudiness are observed in association with the Southern Oscillation phenomena. In some areas, cloudiness shifts between land and ocean areas on time scales as long as a

season. Such shifts in convection have important implications for the local population on land and also possibly for the global radiation budget. With very accurate seasonal mean radiation budget data the implications of these shifts for the global radiation balance can be studied in detail.

Considerable interannual variability also occurs in the snow cover and sea ice in high latitudes [e.g., *Kukla and Kukla*, 1974]. The precise magnitude of the effect of the ice-albedo feedback on the net radiation remains uncertain [e.g., *Lian and Cess*, 1977]. Comparison of accurately measured radiation budget components in a particular region and during a particular season, but for years with differing amounts of snow cover, would provide a fairly unambiguous estimate of the effect of snow cover on the radiation balance.

Many more potential uses of natural interannual variability as a tool for understanding natural climate can be imagined, but an adequate data set for such studies is not currently available. Moreover, there is no indication that an adequate data set will become available in the foreseeable future. The NOAA radiometer data set is approaching the length of record required (around 10 years), but the NOAA data are not broadband measurements. The NOAA albedos are visible albedos which greatly overestimate the broadband albedo of snow, ice, and clouds and underestimate the albedos of vegetation and soils. The NOAA estimates of long-wave emission are estimated from radiance measurements in the window region and are also unsuitable for making subtle comparisons. What is needed is a long, homogeneous record of accurate broadband measurements of the earth's radiation budget with good spatial resolution. ERBE data, even in combination with earlier data, will not provide a record of sufficient temporal extent to exploit the opportunities provided by the interannual variability of the climate.

Acknowledgments. The authors are very grateful to the other members of the ERBE science team for their encouragement and sharing of ideas. R. Kandel, E. Raschke, and E. Harrison provided particularly detailed and useful criticisms of early drafts.

REFERENCES

Albright, M. D., E. E. Recker, R. J. Reed, and R. Dang, The diurnal variation of deep convection and precipitation in the central tropical Pacific during January–February 1979, *Mon. Weather Rev., 113*, 1663–1680, 1984.

Briegleb, B., and V. Ramanathan, Spectral and diurnal variations in clear-sky planetary albedo, *J. Clim. Appl. Meteorol., 21*, 1160–1171, 1982.

Campbell, G. G., and T. H. Vonder Haar, Climatology of radiation budget measurements from satellites, *Atmos. Sci. Pap. 323*, Colo. State Univ., Fort Collins, 1980.

Carbon Dioxide Assessment Committee, *Changing Climate*, 496 pp., National Academy Press, Washington, D. C., 1983.

Cess, R. D., Climate change: An appraisal of atmospheric feedback mechanisms employing zonal climatology, *J. Atmos. Sci., 33*, 1831–1843, 1976.

Cess, R. D., and V. Ramanathan, Averaging of infrared cloud opacities for climate modeling, *J. Atmos. Sci., 35*, 919–922, 1978.

Cess, R. D., B. P. Briegleb, and M. S. Lian, Low-latitude cloudiness and climate feedback: Comparative estimates from satellite data, *J. Atmos. Sci., 39*, 53–59, 1982.

Charlock, T. P., and V. Ramanathan, The albedo field and cloud radiative forcing produced by a general circulation model with internally generated cloud optics, *J. Atmos. Sci., 42*, 1408–1429, 1985.

Charney, J. G., Dynamics of deserts and drought in the Sahel, *Q. J. R. Meteorol. Soc., 101*, 193–202, 1975.

Cubasch, U., Comparison of the influence of different radiation parameterizations on 10 day forecast, in *Workshop on Radiation and Cloud Radiation Interaction in Numerical Modeling*, Eur. Cent. for Medium Range Weather Forecasting, Reading, England, 1981.

Davies, R., The effect of finite geometry on the three dimensional transfer of solar irradiance in clouds, *J. Atmos. Sci., 35*, 1712–1725, 1978.

Duvel, J.-P., and R. S. Kandel, Anisotropy of long-wave radiation emergent from a broken cloud field and its effect on satellite estimates of flux, *J. Clim. Appl. Meteorol., 23*, 1411–1420, 1984.

Duvel, J.-P., and R. S. Kandel, Regional-scale diurnal variations of outgoing infrared radiation observed by Meteosat, *J. Clim. Appl. Meteorol., 24*, 335–349, 1985.

Ellingson, R. G., On the effects of cumulus dimensions on long-wave irradiance and heating rate calculations, *J. Atmos. Sci., 39*, 886–896, 1982.

Ellingson, R. G., and J. C. Gille, An infrared radiative transfer model, 1, Model description and comparison of observations with calculations, *J. Atmos. Sci., 35*, 523–545, 1978.

Ellis, J. S., Cloudiness, the planetary radiation budget and climate, Ph.D. thesis, 129 pp., Colo. State Univ., Boulder, 1978.

Ellis, J. S., and T. H. Vonder Haar, Zonal average earth radiation budget measurements from satellites for climate studies, *Atmos. Sci. Rep. 240*, Dep. of Atmos. Sci., Colo. State Univ., Fort Collins, 1976.

England, C., and G. E. Hunt, Studies of the spatial and temporal errors in satellite estimates of the earth's radiation budget, *Tellus, Ser. B, 36*, 303–316, 1984.

Geleyn, J. F., A. Hense, and H. J. Preuss, A comparison of model generated radiation fields with satellite measurements, *Contrib. Atmos. Phys., 55*, 253–286, 1982.

Gill, A. E., and E. M. Rasmusson, The 1982–83 anomaly in the equatorial Pacific, *Nature, 306*, 229–234, 1983.

Griffith, K. T., S. K. Cox, and R. G. Knollenberg, Infrared radiative properties of tropical cirrus clouds inferred from aircraft measurements, *J. Atmos. Sci., 37*, 1077–1087, 1980.

Gruber, A., Determination of the earth-atmosphere radiation budget from NOAA satellite data, *NOAA Tech. Rep.*, Natl. Environ. Satell. Serv., Washington, D. C., 1978.

Gruber, A., and A. F. Krueger, The status of the NOAA outgoing longwave radiation data set, *Bull. Am. Meteorol. Soc., 65*, 958–962, 1984.

Gruber, A., and J. S. Winston, Earth-atmosphere radiative heating based on NOAA scanning radiometer measurements, *Bull. Am. Meteorol. Soc., 59*, 1570–1573, 1978.

Gruber, A., I. Ruff, and C. Earnest, Determination of the planetary radiation budget from TIROS-N satellites, *NOAA Tech. Rep. NESDIS-3*, Natl. Oceanic and Atmos. Admin., Washington, D. C., 1983.

Gube, M., Radiation budget parameters at the top of the earth's atmosphere derived from Meteosat data, *J. Clim. Appl. Meteorol., 21*, 1907–1921, 1982.

Hansen, J., A. Lacis, D. Rind, G. Russell, P. Stone, I. Fung, J. Lerner, and R. Ruedy, Climate sensitivity: Analysis of feedback mechanisms, in *Climate Processes and Climate Sensitivity, Geophys. Monogr. Ser.*, vol. 29, edited by J. E. Hansen, and T. Takahashi, pp. 130–163, AGU, Washington, D. C., 1984.

Harshvardhan, J. A. Weinman, and R. Davies, Transport of infrared radiation in cuboidal clouds, *J. Atmos. Sci., 38*, 2500–2513, 1981.

Hartmann, D. L., On the role of global-scale waves in ice-albedo and vegetation-albedo feedback, in *Climate Processes and Climate Sensitivity, Geophys. Monogr. Ser.*, vol. 29, edited by J. E. Hansen and T. Takahashi, pp. 18–28, AGU, Washington, D. C., 1984.

Hartmann, D. L., and D. A. Short, On the use of earth radiation budget statistics for studies of clouds and climate, *J. Atmos. Sci., 37*, 1233–1250, 1980.

Hartmann, D. L., H. H. Hendon, and R. A. Houze, Jr., Some implications of the mesoscale circulations in tropical cloud clusters for large-scale dynamics and climate, *J. Atmos. Sci., 41*, 113–121, 1984.

Hastenrath, S., On meridional heat transports in the world ocean, *J. Phys. Oceanogr., 12*, 922–927, 1982.

Hays, J. D., J. Imbrie, and N. J. Shackleton, Variations in the earth's orbit: Pacemaker of the ice ages, *Science, 194*, 1121–1132, 1976.

Heddinghaus, T. R., and A. F. Krueger, Annual and interannual variations in outgoing longwave radiation over the tropics, *Mon. Weather Rev., 109*, 1208–1218, 1981.

Hunt, B. G., On the general circulation of the atmosphere without clouds, *Q. J. R. Meteorol. Soc., 104*, 91–102, 1978.

Hunt, G. E., Radiative properties of terrestrial clouds at visible and infrared thermal window wavelengths, *Q. J. R. Meteorol. Soc., 99*, 346–369, 1973.

Imbrie, J., and J. Z. Imbrie, Modeling the climatic response to orbital variations, *Science, 207*, 943–953, 1980.

Jacobowitz, H., N. L. Smith, H. B. Howell, F. W. Nagle, and J. R. Hickey, The first 18 months of planetary radiation budget measurements from the Nimbus 6 ERB experiment, *J. Atmos. Sci., 36*, 501–507, 1979.

Jacobowitz, H., R. J. Tighe, and Nimbus 7 ERB Experiment Team, The earth radiation budget derived from the Nimbus 7 ERB experiment, *J. Geophys. Res.*, *89*, 4997–5010, 1984.

Kandel, R., Satellite observation of the earth radiation budget, *Contrib. Atmos. Phys.*, *56*, 322–340, 1983.

Kukla, G. J., and H. J. Kukla, Increased surface albedo in the northern hemisphere, *Science*, *183*, 709–714, 1974.

Lau, K. M., and P. M. Chan, Short term climate variability and atmospheric teleconnection from satellite-observed outgoing longwave radiation, I and II, *J. Atmos. Sci.*, *40*, 2735–2767, 1983.

Lian, M. S., and R. C. Cess, Energy balance climate models: A reappraisal of ice-albedo feedback, *J. Atmos. Sci.*, *34*, 1048–1062, 1977.

Liebmann, B., and D. L. Hartmann, Interannual variations of outgoing IR associated with tropical circulation changes during 1974–78, *J. Atmos. Sci.*, *39*, 1153–1162, 1982.

Liebmann, B., and D. L. Hartmann, An observational study of tropical-midlatitude interaction on intraseasonal time scales during winter, *J. Atmos. Sci.*, *41*, 3333–3350, 1984.

Liou, K.-N., and Q. Zheng, A numerical experiment on the interactions of radiation, clouds and dynamic processes in a general circulation model, *J. Atmos. Sci.*, *41*, 1513–1535, 1984.

London, J., A study of the atmospheric heat balance, report, contract AF 19(122)-165, Coll. of Eng., New York Univ., New York, 1957.

Manabe, S., and R. T. Wetherald, Thermal equilibrium of the atmosphere with a given distribution of relative humidity, *J. Atmos. Sci.*, *24*, 241–259, 1967.

McKee, T. B., and S. K. Cox, Scattering of visible radiation by finite clouds, *J. Atmos. Sci.*, *31*, 1885–1892, 1974.

Milankovitch, M., *Théorie Mathématique des Phénomènes Thermiques Produits par la Radiation Solaire*, 339 pp., Gauthier-Villars, Paris, 1920.

Minnis, P., and E. F. Harrison, Diurnal variability of regional cloud and clear-sky radiative parameters derived from GOES data, I, Analysis method, *J. Clim. Appl. Meteorol.*, *23*, 993–1011, 1984*a*.

Minnis, P., and E. F. Harrison, Diurnal variability of regional cloud and clear-sky radiative parameters derived from GOES data, II, November 1978 cloud distributions, *J. Clim. Appl. Meteorol.*, *23*, 1012–1031, 1984*b*.

Minnis, P., and E. F. Harrison, Diurnal variability of regional cloud and clear-sky radiative parameters derived from GOES data, III, November 1978 radiative parameters, *J. Clim. Appl. Meteorol.*, *23*, 1032–1051, 1984*c*.

Mintz, Y., The sensitivity of numerically simulated climates to land-surface boundary conditions, in *The Global Climate*, edited by J. T. Houghton, pp. 79–106, Cambridge University Press, New York, 1984.

Morcrette, J. J., and J. F. Geleyn, On the influence of different radiation parameterizations on model generated fields, *Q. J. R. Meteorol. Soc.*, *111*, 565–585, 1985.

Murakami, T., Temporal variations of satellite observed outgoing longwave radiation over the winter monsoon region, I, Long period (15–30) oscillations, *Mon. Weather Rev.*, *108*, 408–426, 1980.

North, G. R., R. F. Cahalan, and J. A. Coakley, Jr., Energy balance climate models, *Rev. Geophys.*, *19*, 91–121, 1981.

Oerlemans, J., and H. M. Van den Dool, Energy balance climate models: Stability experiments with a refined albedo and updated coefficients for infrared emission, *J. Atmos. Sci.*, *35*, 371–381, 1978.

Ohring, G., and P. F. Clapp, The effect of changes in cloud amount on the net radiation at the top of the atmosphere, *J. Atmos. Sci.*, *37*, 447–454, 1980.

Ohring, G., and A. Gruber, Satellite radiation observations and climate theory, *Adv. Geophys.*, *25*, 237–304, 1983.

Ohring, G., P. F. Clapp, T. R. Heddinghaus, and A. F. Krueger, The quasi-global distribution of the sensitivity of earth-atmosphere radiation budget to clouds, *J. Atmos. Sci.*, *38*, 2539–2541, 1981.

Oort, A. H., Global atmospheric circulation statistics, 1958–1973, *NOAA Prof. Pap. 14*, 180 pp., U.S. Gov. Print. Office, Washington, D. C., 1983.

Oort, A. H., and T. H. Vonder Haar, On the observed annual cycle in the ocean-atmosphere heat balance over the northern hemisphere, *J. Phys. Oceanogr.*, 781–800, 1976.

Oxford GARP Study Conference, *Parameterization of Extended Cloudiness and Radiation for Climate Models*, pp. 1–50, Global Atmospheric Research Program, World Meteorological Organization, Geneva, 1979.

Pinker, R. T., J. A. Ewing, and J. D. Tarpley, Interdependence of the planetary and surface net radiation, *J. Clim. Appl. Meteorol.*, *24*, 1262–1268, 1985.

Ramanathan, V., E. J. Pitcher, R. C. Malone, and M. L. Blackmon, The response of a spectral general circulation model to refinements in radiative processes, *J. Atmos. Sci.*, *40*, 605–630, 1983.

Randall, D. A., J. A. Abeles, and T. G. Corsetti, Seasonal simulations of the planetary boundary layer and boundary-layer stratocumulus clouds with a general circulation model, *J. Atmos. Sci.*, *42*, 641–676, 1985.

Raschke, E., and W. R. Bandeen, The radiation balance of the planet earth from radiation measurements of the satellite Nimbus II, *J. Clin. Appl. Meteorol.*, *9*, 215–238, 1970.

Raschke, E., T. H. Vonder Haar, W. R. Bandeen, and M. Pasternak, The annual radiation balance of the earth-atmosphere system during 1969–1970 from Nimbus 3 measurements, *J. Atmos. Sci.*, *30*, 341–364, 1973.

Rasmusson, E. M., and J. M. Wallace, Meteorological aspects of the El Nino/Southern Oscillation, *Science*, *222*, 1195–1202, 1983.

Rasool, S. I., On dynamics of deserts and climate, in *The Global Climate*, edited by J. T. Houghton, pp. 107–120; Cambridge University Press, New York, 1984.

Schiffer, R. A., and W. B. Rossow, The International Satellite Cloud Climatology Project (ISCCP): The first project of the World Climate Research Programme, *Bull. Am. Meteorol. Soc.*, *64*, 779–784, 1983.

Schneider, S. H., Cloudiness as a global climate feedback mechanism: The effects on the radiation balance and surface temperature of variations in cloudiness, *J. Atmos. Sci.*, *29*, 1413–1422, 1972.

Schneider, S. H., and C. Mass, Volcanic dust, sunspots and temperature trends, *Science*, *190*, 741–746, 1975.

Schneider, S. H., W. M. Washington, and R. M. Chervin, Cloudiness as a climate feedback mechanism: Effects on cloud amounts of prescribed global and regional surface temperature changes in the NCAR GCM, *J. Atmos. Sci.*, *35*, 2207–2221, 1978.

Shine, K. P., A. Henderson-Sellers, and A. Slingo, The influence of the spectral response of satellite sensors on estimates of broadband albedo, *Q. J. R. Meteorol. Soc.*, *110*, 1170–1179, 1984.

Short, D. A., and R. F. Cahalan, Interannual variability and climatic noise in satellite observed outgoing longware radiation, *Mon. Weather Rev.*, *111*, 572–577, 1983.

Short, D. A., and J. M. Wallace, Satellite inferred morning to evening cloudiness changes, *Mon. Weather Rev.*, *108*, 1160–1169, 1980.

Short, D. A., G. R. North, T. D. Bess, and G. L. Smith, Infrared parameterization and simple climate models, *J. Clim. Appl. Meteorol.*, *23*, 1222–1233, 1984.

Shukla, J., and Y. Sud, Effect of cloud-radiation feedback on the climate of a general circulation model, *J. Atmos. Sci.*, *38*, 2337–2353, 1981.

Slingo, A., and H. M. Schrecker, On the shortwave radiation properties of stratiform water clouds, *Q. J. R. Meteorol. Soc. 108*, 407–426, 1982.

Slingo, A., S. Nicholls, and J. Schmetz, Aircraft observations of marine stratocumulus during JASIN, *Q. J. R. Meteorol. Soc.*, *108*, 833–856, 1982.

Slingo, J., A study of the earth's radiation budget using a general circulation model, *Q. J. R. Meteorol. Soc.*, *108*, 379–405, 1982.

Smith, E. A., T. H. Vonder Haar, J. R. Hickey, and R. Maschoff, The nature of the short period fluctuations in solar irradiance received by the earth, *Clim. Change*, *5*, 211–235, 1983.

Stephens, G. L., Radiation profiles in extended water clouds, II, Parameterization schemes, *J. Atmos. Sci.*, *35*, 2123–2132, 1978.

Stephens, G. L., G. G. Campbell, and T. H. Vonder Haar, Earth radiation budget measurements from satellites and their interpretation for climate modeling and studies, *J. Geophys. Res.*, *86*, 9739–9760, 1981.

Street-Perrott, F. A., and S. P. Harrison, Temporal variations in lake levels since 30,000 yr BP: An index of the global hydrological cycle, in *Climate Processes and Climate Sensitivity*, *Geophys. Monogr. Ser.*, vol. 29, edited by J. E. Hansen and T. Takahashi, pp. 118–129, AGU, Washington, D. C., 1984.

van Loon, H., Cloudiness and precipitation in the southern hemisphere, *Meteorol. Monogr.*, *13*, 101–111, 1972.

Vonder Haar, T. H., Climate studies from satellite observations: Special problems in the verification of earth radiation balance, cloud climatology, and related climate experiments, *Adv. Space Phys.*, *2*, 3–10, 1983.

Vonder Haar, T. H., and A. H. Oort, New estimate of annual poleward energy transport by northern hemisphere oceans, *J. Phys. Oceanogr.*, *2*, 169–172, 1973.

Warren, S. G., and S. H. Schneider, Seasonal simulation as a test for uncertainties in the parameterization of a Budyko-Sellers zonal climate model, *J. Atmos. Sci.*, *36*, 1377–1391, 1979.

Warren, S. G., and S. L. Thompson, The climatological minimum in

tropical outgoing infrared radiation: Contributions of humidity and clouds, *Q. J. R. Meteorol. Soc.*, *109*, 169–185, 1983.

Weickmann, K. M., Intraseasonal fluctuations in near-global-scale modes of circulation and outgoing longwave radiation during northern hemisphere winter, *Mon. Weather Rev.*, *111*, 1838–1858, 1983.

Wetherald, R. T., and S. Manabe, Cloud cover and climate sensitivity, *J. Atmos. Sci.*, *37*, 1485–1510, 1980.

Willson, R. C., S. Gulkis, M. Jansen, N. S. Hudson, and G. A. Chapman, Observations of solar irradiance variability, *Science*, *211*, 700–702, 1981.

Winston, J. S., A. Gruber, T. I. Gray, M. S. Varnadore, C. L. Earnest, and L. P. Manello, Earth atmosphere radiation budget derived from NOAA satellite data, June 74–Febr. 78, *Rep. NOAA S/T 79-187*, vol. 1 and 2, Natl. Oceanic and Atmos. Admin., Washington, D. C., 1979.

World Climate Program, The ISCCP preliminary implementation plan (revision 1), *Rep. WCP-35*, World Meteorol. Organ., Geneva, 1982.

Zdunkowski, W. G., and W. K. Crandall, Radiative transfer of infrared radiation in model clouds, *Tellus*, *23*, 517–527, 1971.

A. Berroir, Institut National des Sciences de l'Univers/CNRS, 77 avenue Denfert Rochereau, 75014 Paris, France.

D. L. Hartmann, Department of Atmospheric Sciences, University of Washington, Seattle, WA 98195.

G. E. Hunt, Centre for Remote Sensing, Imperial College of Science and Technology, London SW7 2BZ, England.

V. Ramanathan, Climate Sensitivity Group, National Center for Atmospheric Research, Boulder, CO 80307.

(Received March 4, 1985;
accepted October 2, 1985.)